HHS Public Access

Author manuscript

Sci Transl Med. Author manuscript; available in PMC 2022 October 10.

Published in final edited form as:

Sci Transl Med. 2022 January 05; 14(626): eabg0253. doi:10.1126/scitranslmed.abg0253.

Distinct populations of highly potent TAU seed conformers in rapidly progressing Alzheimer's disease

Chae Kim[1], **Tracy Haldiman**[1], **Sang-Gyun Kang**[2], **Lenka Hromadkova**[1], **Zhuang Zhuang Han**[2], **Wei Chen**[1,3], **Frances Lissemore**[4], **Alan Lerner**[4], **Rohan de Silva**[5], **Mark L. Cohen**[1,3], **David Westaway**[2], **Jiri G. Safar**[1,4,*]

[1]Department of Pathology, Case Western Reserve University School of Medicine, Cleveland, OH 44106, USA

[2]Centre for Prions and Protein Folding Diseases, University of Alberta, Edmonton T6G 2M8, Canada

[3]National Prion Disease Pathology Surveillance Center, Case Western Reserve University School of Medicine, Cleveland, OH 44106, USA

[4]Department of Neurology, Case Western Reserve University School of Medicine, Cleveland, OH 44106, USA

[5]Reta Lila Weston Institute of Neurological Studies and Department of Molecular Neuroscience, UCL Institute of Neurology, London WC1N 1PJ, UK

Abstract

Although genetic factors play a main role in determining the risk of developing Alzheimer's disease (AD), they do not explain extensive spectrum of clinicopathological phenotypes. Deposits of aggregated TAU proteins are one of the main predictors of cognitive decline in AD. We investigated the hypothesis that variabilities in AD progression could be due to diverse structural assemblies (strains) of TAU protein. Using sensitive biophysical methods in 40 patients with AD and markedly different disease durations, we identified populations of distinct TAU particles that differed in size, structural organization, and replication rate in vitro and in cell assay. The

*Corresponding author. jiri.safar@case.edu.

Author contributions: J.G.S. and D. W. conceived the study. M.L.C. performed diagnostic neuropathology. A.L. and F.L. collected, processed, and interpreted clinical data. C.K. conducted conformational and sucrose gradient analyses. T.H. expressed and purified recombinant K18 and K19 TAU proteins and performed seeding assays. W.C. performed prion protein analyses and immunohistochemistry. J.G.S., C.K., T.H., L.H., and D.W. designed the experiments and interpreted and prepared the data for publication. J.G.S. wrote the paper, and all authors were involved in reviewing, refining, and approving the final version of the manuscript.

Competing interests: The authors declare that they have no competing financial interests.

SUPPLEMENTARY MATERIALS

www.science.org/doi/10.1126/scitranslmed.abg0253

Materials and Methods

Figs. S1 to S6

Tables S1 and S2

Materials Design Analysis Reporting (MDAR) Checklist for Authors

References (101–114)

View/request a protocol for this paper from Bio-protocol.

rapidly replicating, distinctly misfolded TAU conformers found in rapidly progressive AD were composed of ~80% misfolded four-repeat (4R) TAU and ~20% of misfolded 3R TAU isoform with the same conformational signatures. These biophysical observations suggest that distinctly misfolded population of 4R TAU conformers drive the rapid decline in AD and imply that effective therapeutic strategies might need to consider not a singular species but a cloud of differently misfolded TAU conformers.

Shape matters

The accumulation of TAU protein aggregates is one of the major hallmarks of Alzheimer's disease (AD). Although TAU accumulation has been shown to be a predictor of cognitive decline in patients with AD, the correlation between AD progression and TAU remains to be elucidated. Here, Kim et al. isolated and analyzed TAU protein structure obtained from patients with different disease progression and showed an association between progression rate and distinct TAU conformers. Rapidly progressing AD was associated with mostly misfolded four-repeat (4R) TAU and high replication rate in vitro. The results suggest that the structure of TAU protein aggregates should be considered when developing potential treatment for slowing or halting AD progression.

INTRODUCTION

The genetic and environmental factors linked to the increased risk of developing late-onset Alzheimer's disease (AD) are well established, but they explain only ~30% of phenotypic variability (1, 2). We recently described a subgroup of patients with rapidly progressive dementia mimicking prion diseases, which, after exhaustive neuropathological investigation and prion protein gene sequencing, was concluded to be the rapidly progressive AD (rpAD) (3). Data from all of the rpAD cases collected independently at prion centers in Germany, Japan, Spain, and France have uniformly confirmed the presence of differentiating clinical characteristics and a low frequency of e4 alleles in the *APOE* gene, whereas the autosomal dominant history of dementia or comorbidity was absent (4–9). The high concentrations of distinctly folded conformers of amyloid β with extended C termini (Aβ42) that we found in rpAD (9) were confirmed by nuclear magnetic resonance spectroscopy (10). This suggests critical differences in the pathogenesis of rpAD, but the molecular mechanism of rapid progression is not completely understood (11).

Recent evidence suggests that AD is a dual proteinopathy in which Aβ deposition and the accumulation of aggregated TAU drive AD pathogenesis. However, deposits of abnormal TAU protein seem to be the critical factor in determining cognitive decline (12). Extensive analysis of aging brain samples indicates that the pathological processes underlying AD begin early with depositing aggregates of hyperphosphorylated TAU protein in isolated anatomical structures of the brain and then spread through neuronal projections (13). An accumulation of data from cell and transgenic mice models suggests that different TAU aggregates generated in vitro or in vivo can replicate in cells, accelerate, and propagate the formation of TAU aggregates in transgenics, thus suggesting a prion-like phenomenon (14, 15). The discovery that misfolded prion proteins can replicate in the absence of informative nucleic acid represented a new biological paradigm. This is now supported by many lines

of evidence from biochemical, genetic, and animal studies (16–20), by in vitro synthesis of mice and hamster prions (21–27), and lastly by generation of synthetic human prions from recombinant protein expressed in bacteria (28). The discovery of Ure 3 and Sup35 yeast prions expanded this paradigm to include cytoplasmic proteins that are phylogenetically very distant from prion protein (29, 30).

Apart from distinct clinical and neuropathological phenotype in the original host, the generally accepted criterion for the detection and differentiation of distinct human prion strains derived from the study of Creutzfeldt-Jakob disease are differential conformational characteristics of prion protein determined with sensitive biophysical tools (28). Although the extent to which data from tauopathy models and in vitro generated TAU aggregates fulfill these criteria is vigorously debated, these findings have raised some fundamental questions, specifically, whether the structure of different conformers and assemblies of brain TAU contribute to varying progression rates of AD and whether subtle differences in the conformation of TAU are responsible for the distinct disease phenotypes (31).

By adapting advanced conformation-sensitive biophysical techniques originally developed for strain typing of human prions (32–34), we investigated the structural organization of different isoforms of TAU protein in the hippocampus of 40 AD cases with variable progression rate. The hippocampus is considered critical in cognitive decline and a crossroad in the spread of pathogenic TAU aggregates, from early deposits in transentorhinal cortex (Braak stages I and II) to major projections to the hippocampus where TAU pathology gradually advances into CA1 region (Braak II), followed by spread to the limbic structures, inferior temporal neocortex (Braak III), and the amygdala and thalamus (Braak IV) and lastly spreading into the neocortex (Braak V and VI) (13, 14). Our findings demonstrate a structural diversity of hippocampal TAU and establish a link between particular conformers (strains) of misfolded TAU protein, their replication in vitro, and the progression rate of AD.

RESULTS

Comparative demographics, neuropathology, and *APOE* allelic frequency in rapidly and slowly progressive AD

The rapidly progressive cases of AD were initially referred to the National Prion Disease Pathology Surveillance Center as rapidly progressive or atypical dementia with working diagnosis of probable prion diseases, which subsequently failed to show neuropathologic or genetic evidence of prion disease after *PRNP* gene sequencing and instead demonstrated National Institute of Aging–Alzheimer's Association (NIA-AA) neuropathological criteria for definite AD (35). Of 186 cases with an identifiable disease starting date gathered from detailed clinical records and semistructured telephone interviews of patient and/or caregivers at the time of referral, we selected cases with available frozen hippocampal tissue. Our second cohort consisted of classical AD cases collected at the Case Western Reserve University (CWRU) Memory and Aging Center (see Materials and Methods) that matched the progression rates and demographics distribution in the National Alzheimer's Coordinating Center (NACC) dataset and hereafter was referred to as slowly progressive AD (spAD) (Fig. 1 and table S1). Because there is no single clinical criterion differentiating rpAD from spAD, we used the decline in more than six Mini-Mental State Examination

(MMSE) points per year and, in cases with no available MMSE, the 3-year disease duration alone. The MMSE criterion strongly correlates with death within 3 years of initial neurological diagnosis of atypical dementia (table S1) (7–9, 36), and the about sixfold faster progression in rpAD cases was associated with younger age at death (Fig. 1, A and B) and low frequency of *APOE* gene e4 allele (Fig. 1C and table S1). These data agree with findings from previous studies (8, 9, 37) and data from prion centers in Japan and Europe (4). Neuropathological evaluation according to the NIA-AA guidelines (35) showed no differences in the severity of pathology between rpAD and spAD using NIA-AA scale (Fig. 1D and table S1), including hippocampal pathology of TAU monitored with monoclonal antibody AT8 immunohistochemistry (Fig. 1, E and F) and evaluated according to Braak (13) (B parameter in table S1). In hippocampus, we observed extensive variations and no statistical differences in denatured/native (D/N) ratio and concentration of Aβ 1-40 (Aβ40) and 1-42 (Aβ42) between rpAD and spAD, in contrast to major differences in Aβ42 conformation that we detected previously in precuneus/posterior cingulate cortex (fig. S1A and table S1) (9). Cumulatively, the neuropathological findings in rpAD are consistent with NIA-AA diagnostic classification of AD, and occurrence of these rapidly progressive cases in prion centers across various methodologies, populations, and health care systems is evidence for a distinct and more severe form of sporadic AD, this being associated with a low frequency of e4 allele of the *APOE* gene that is similar to the general healthy population (4, 5, 7–9, 37–40).

Concentration and conformation of three- and four-repeat TAU isoforms in different phenotypes of AD

Because the data failed to support varying TAU neuropathological markers as a denominator of rapid cognitive decline in rpAD (table S1), we hypothesized that TAU misfolding could generate different conformers of misfolded TAU (strains) that, in turn, could affect cognitive decline. Accordingly, we adapted conformation-dependent immunoassays (CDIs) and conformational stability assays (CSAs) (34, 41). In CDI, we use the europium-labeled monoclonal antibody (mAb) against epitopes that are hidden under native conditions and are exposed only after denaturation with strong chaotropes such as Gdn HCl (34, 41). The CSA involves the use of incremental Gdn HCl concentrations to progressively unfold the misfolded protein, and differences in stability profiles have provided evidence for distinct conformations of prion, Aβ, and, most recently, P301L TAU strains (9, 32–34, 40–43). Both CDI ratios and CSA conformational signatures are independent of the absolute concentrations of the misfolded protein and do not require an in vitro amplification step or purification before detection: procedures that can change the in vivo conformational repertoire and biological properties of strain isolates (28, 44). The data for human and animal-adapted prions indicate that CSAs differentiate strain signatures regardless of posttranslational modifications including glycosylation and glycolipidation (9, 28, 32, 43, 45–47), and we selected for conformational monitoring mAb with epitopes in TAU domains less decorated by posttranslational modifications, mAb 77G7 specific for R3/4 boundary in both three-repeat (3R) and 4R microtubule binding repeats (41) and mAb repeat domain 3 (RD3) specific for the R1/R3 repeat boundary of the 3R TAU isoform (2N3R) (Fig. 1G) (48–50). Europium-labeled detection 77G7 and RD3 or the capture monoclonal antibody DA9 mAbs do not have conformational epitopes and detect only open (linear and unfolded)

conformers of monomeric TAU because it has been shown with 77G7 mAb in misfolded P301L TAU in human frontotemporal lobar degeneration (FTLD) and in a corresponding transgenic mouse model (41). In addition, all antibodies have epitopes outside known phosphorylation sites in paired helical filaments (PHFs) and acetylated Lys^{174}, Lys^{274}, and Lys^{280} that have been described in the TAU deposits of patients with AD, FTLD-MAPT, and Pick's disease (51–53). Using denatured TAU410 and TAU441 as calibrants, the Eu-labeled RD3 demonstrated high sensitivity and specificity for TAU410 and up to four orders of magnitude linearity range and with ≤5% cross-reactivity with TAU441 (fig. S1, B and C).

We assessed a set of hippocampal samples from definite AD cases with diverse duration of disease and age of death (table S1). CDI and immunohistochemistry for Aβ, α-synuclein, TDP-43, and FUS excluded coexistent proteinopathies and other comorbidities (9, 54). Noting these data, we examined the sarkosyl-insoluble total TAU in the hippocampus of all AD cases (Fig. 2, A and B). Although the concentrations of sarkosyl-insoluble TAU aggregates did not correlate with disease progression (Fig. 2A), the CDI D/N ratio after proteinase K (PK) treatment showed a highly significant ($P = 0.002$) correlation with the disease duration (Fig. 2B), suggesting that distinct conformers of TAU might be involved in determining disease progression. In addition, comparing the concentration of sarkosyl-insoluble TAU did not show differences between AD cases, and both rpAD ($P = 0.002$) and spAD ($P = 0.010$) accumulated significantly more TAU aggregates compared to age-matched controls (Fig. 2C). Both rpAD and spAD cases had a significantly ($P < 0.001$) higher D/N ratio of both total and 3R TAU when compared with controls, and rpAD cases accumulated total TAU with higher D/N ratio than spAD cases (Fig. 2D); the D/N ratio for 3R TAU was not different (Fig. 2D). Assessing the concentrations of 4R and 3R TAU as a percentage of total TAU showed broad interindividual values in soluble TAU fractions but consistently higher fraction of 4R TAU in the insoluble TAU aggregates (Fig. 2E). The spread of data is evidence of extensive interindividual variability of insoluble TAU concentrations in both rpAD and spAD groups. Nevertheless, the concentration-independent CDI D/N ratios show significant differences in conformations of insoluble ($P = 0.022$; Fig. 2D) and protease resistant ($P = 0.003$) TAU in the rpAD cohort (Fig. 2F). These results suggest that distinct conformers formed mostly from protease-resistant 4R TAU are associated with rapid progression of AD.

Size, isoform composition, and conformation of misfolded TAU aggregates in AD

To investigate the size and composition of misfolded brain-derived TAU aggregates without confounding purification or chemical processing steps, we adopted high-speed velocity sedimentation profiling in nondenaturing sucrose gradients, which provides fundamental information about the size, composition, and infectivity of human brain-derived prions in Creutzfeldt-Jakob disease and animal models (32, 55). Using hippocampal samples, the top fractions of these sucrose gradients were found to be mixtures of both 3R and 4R TAU in both rpAD and spAD (Fig. 3, A to D). These TAU isoforms were monomers with an open conformation in both rpAD and spAD, as indicated by D/N ratio ~1 due to equal exposure of both N terminus and RD in native and denatured states (Fig. 3, E and F). The aggregates of brain-derived TAU demonstrated a range of sedimentation velocities, from small aggregates with low sedimentation velocity formed by about four TAU monomers up to the most

frequent large aggregates, which were composed of ~120 monomers of TAU (Fig. 3, A to D). In both rpAD and spAD, the most abundant aggregates are, regardless of size, formed from 78 to 86% of 4R TAU and 12 to 23% of 3R TAU. There was a discontinuity wherein the highest D/N ratio is shifted to fraction 3 with smaller aggregates (Fig. 3, E and F) from the most abundant larger aggregates in fraction 2 (Fig. 3, A and B), indicating distinct sets of conformations in fractions 1, 2, 3, and 4 (Fig. 3, A and E). Cumulatively, the sucrose gradient velocity sedimentation experiments indicate that misfolded TAU conformers are composed of predominantly 4R TAU and that they are not a singular particle but represent a broad range of sizes and conformations.

Conformational diversity of 4R and 3R TAU in patients with AD

Total TAU in hippocampus of individual patients yielded complex CSA profiles with 50% of TAU conformers unfolding [as indicated by fractional change of unfolding (F_{app}) values of 0.5] between 1.2 and 2.3 M Gdn HCl, with major peaks at ~2 M Gdn HCl, followed by complete unfolding above 3 M Gdn HCl; the patterns of unfolding in rpAD and spAD were similar (Fig. 4, A and B). The RD3 antibody demonstrated with monomers of Tau K19 (3R) a CSA signal that did not change with increasing Gdn HCl concentration and thus resulted in a D/N ratio of ~1, as expected for an open (unfolded, unstructured) (56) TAU state (fig. S1F). A similar observation was previously shown with recombinant monomers of 2N4R TAU441 (41). In contrast, the K19 fibrils that sedimented to the bottom of sucrose gradient (fig. S1E) showed a high D/N ratio and sigmoidal transition from native to unfolded state (fig. S1F). Accordingly, the D/N ratios of Tau 1.9 ± 0.4 (mean ± SD) with mAb Eu-77G7 and 1.5 ± 0.1 with Eu-RD3 in non-neurological controls (Fig. 2D) indicate comparable exposure of both 77G7 and RD3 epitopes in 4R and 3R TAU in native and denatured states, respectively. In addition, the top sucrose fraction containing soluble monomers of 4R and 3R Tau had a D/N ratio of 1.3 ± 0.3, which documents the corresponding exposure of both RD3 and 77G7 epitopes in native and denatured states and in both rpAD (Fig. 3E) and spAD (Fig. 3F) cases. Cumulatively, the data on soluble 3R and 4R Tau indicate that they exist in the brain as monomers with open (unstructured) native conformation, as expected from in vitro experiments with recombinant analogs (56).

The CSA profiles of 3R TAU with Eu-RD3 antibody generated nearly superimposable profiles to those for total TAU in both rpAD and spAD (figs. S1D and S2, A and B). PK treatment of detergent-insoluble TAU shifted the resulting sigmoidal curves and their midpoints to the higher concentrations of Gdn HCl between 2.0 and 2.6 M Gdn HCl (Fig. 4, C and D), and per the situation for total TAU, the profiles of PK-resistant 3R TAU and total TAU for individual AD cases were indistinguishable (fig. S2, C and D). Performing a subtraction function on the individual curves from the original curves without PK treatment yielded the unfolding profiles for protease-sensitive misfolded total TAU (Fig. 4, E and F) and 3R TAU (fig. S2, E and F). The dip between 2 and 3 M Gdn HCl in some profiles, which is greatly diminished after PK treatment suggests rapid reaggregation of misfolded protease-sensitive TAU conformers during the sample processing. Thus, detergent-insoluble TAU aggregates accumulating in the hippocampus of AD cases encompass a spectrum of distinct conformers within each individual case with abundant protease-sensitive species. That the residual protease-resistant TAU species did not converge to a single overlapping

signature corroborates the conformational diversity of protease-sensitive TAU conformers. The CSA profiles of total, protease-resistant, and protease-sensitive 3R TAU were nearly superimposable with CSA profiles deriving from total TAU (4R + 3R) (Fig. 4 and figs. S1D and S2).

Differential seeding potency of TAU accumulating in the hippocampus of rpAD and spAD cases

Evidence accumulated with prions and, more recently, with a growing list of other proteins indicates that the misfolded conformers can be amplified in vitro in a seeded reaction, a prerequisite step for misfolding propagation in the brain (28, 41, 57–59). To establish the seeding potency and kinetics of misfolded TAU propagation in vitro, we adapted this conformational templating mechanism for amplification of AD brain-derived TAU seeds using recombinant K18 (4R) TAU and K19 (3R) TAU substrates (fig. S3, B to E) (60, 61). Our initial titration experiments of both substrates and low–molecular weight heparin cofactor using a 60-hour experimental window were designed to obviate spontaneous formation of thioflavin T positive aggregates and to obtain maximized responses from homologous brain-derived TAU seeds. As a reference and calibrant, we tested serial dilutions of the prototypical 4R TAU accumulating in the cortex of FTLD-MAPT P301L cases (41) and prototypical 3R TAU Pick's disease (62) in a 96-well format originally designed for amplification of prions (real-time quaking-induced conversion) (59, 63). At the same recombinant K18 and K19 substrate concentrations, the TAU seeds preferentially amplified with homologous substrates and demonstrated end point sensitivity up to 10^{-8} dilution of the brain tissue, corresponding to an average 60 fg of misfolded TAU per well, and lower sensitivity with a stochastic response with nonhomologous substrates (fig. S3, B and E). With K18 (4R) substrate, hippocampal brain homogenates of rpAD cases demonstrated shorter lag phase at 10^{-4} dilution than spAD cases (Fig. 5, A and C), and the differences were highly significant ($P = 0.0002$; Figs. 5E and 6A). In contrast, K19 (3R) substrate showed an overall and extended lag phase in both rpAD and spAD (Fig. 5, B and D), and the difference between rpAD and spAD was not significant (Figs. 5F and 6A). Fitting data to the Hill equation confirmed these observations and demonstrated a generally lower TAU aggregate growth rate constant (r) of rpAD TAU aggregates with K18 substrate versus K19 substrate, which offset the longer lag phases and faster rise times for thioflavin T fluorescence seen for reactions with K19 substrate (Figs. 5 and 6A and table S2). We interpret these data as evidence of broad seeding potency of distinct conformers of TAU in individual AD cases and with more potent seeds accumulating in AD cases with a faster clinical progression. Next, we tested whether the concentration of sarkosyl-insoluble TAU has an impact on lag phase. Figure 6B shows cumulatively a broad spread of both lag phase data against a large variation of sarkosyl-insoluble TAU concentrations, resulting in a lack of correlation in regression analysis. However, the CDI D/N ratio indicates that the lag time in K18 amplification correlates significantly ($P = 0.007$) with the conformation of protease-resistant sarkosyl-insoluble TAU (Fig. 6D). We observed no t correlations for TAU seeding with K19 (3R) substrate before or after protease treatment (Fig. 6, C, E, and F). Cumulatively, the data indicate that the most reliable predictor of seeding activity is not the concentration but the conformation of PK-resistant fraction of insoluble 4R TAU, which, in turn, correlates with faster disease progression (Fig. 2B).

Seeding activity of AD brain-derived TAU measured in cellular assay

We next performed cellular assay for misfolded TAU using human embryonic kidney (HEK) 293T cells expressing TAU 4R RD substrate fragment that includes aggregation-prone mutations (P301L and V337M). The corresponding TAU reporter cells are denoted HEK-TAURD-LM-YFP and were calibrated recently with brain samples from FTLD-MAPT-P301L cases and a cognate mouse transgenic model (41). All the AD brain-derived samples generated a speckled morphology for induced TAU aggregates (Fig. 6G). Because prion-like conformer selection and evolution (64, 65) might occur in the TAU reporter cells due to the permissive nature of the P301L and V337M mutations, we monitored the cells on a daily basis but did not observe any drift in the morphology of induced aggregates. Elevated prion-like seeding activities were detected in all AD brain-derived TAU samples with significantly higher frequency ($P = 0.037$) of positive cells exposed to rpAD TAU, whereas other neurological disease (OND) samples were devoid of speckle-inducing activity (Fig. 6H). We observed an induction of TAU aggregation in cells exposed to AD samples in the first 24 hours, and no TAU aggregation or toxicity was detected with samples from control non-AD cases during 5-day monitoring (Fig. 6, G and H). To address about threefold higher variance (spread) in the percentage of positive cells in rapid AD data when compared with slowly progressive cases, we retested the initial samples after 1 year of storage. The same median and variance values indicate that the cell reporter system and evaluation protocol is highly reproducible (fig. S4) and suggest that the notable spread of positive cell frequency is due to the broader spectrum of seeding-competent TAU conformers in rpAD.

Conformational cloud of misfolded strains of TAU in AD

With the exception of several CSA curves of TAU after PK treatment (Fig. 4, C and D), all other TAU CSA curves were nonsigmoidal, indicating more than a single transition from native to denatured state. We analyzed these profiles using statistical mechanical deconvolution and Gaussian models previously applied to proteins that undergo multistep thermal denaturation (66, 67) and, more recently, to analysis of TAU in FTLD *MAPT* P301L (41). Gaussian deconvolution of averaged profiles in samples with nonsigmoidal TAU denaturation profiles revealed three peaks before protease treatment (Fig. 7, A and B), three or four peaks after PK treatment (Fig. 7, C and D), and, consistently, three peaks in protease-sensitive TAU conformers (Fig. 7, E and F), each representing distinct conformers with different stabilities that unfolded sequentially with Gdn HCl. These data provide direct evidence that each TAU CSA subtype is a mixture of up to four distinct conformers (Fig. 7). Although the conformational profiles of total TAU in rpAD and spAD before PK treatment were similar, the analysis of CSA of protease-resistant TAU revealed significant differences in the profiles at 2.75 M ($P < 0.001$) and 3.25 M Gdn HCl ($P = 0.002$) (Fig. 7, C and D) and the same peaks and scores were found for 3R TAU ($P < 0.001$ and $P = 0.026$, respectively) (fig. S5, C and D). The protease treatment eliminated up to 40% of insoluble TAU conformers, and their lower stability in Gdn HCl (Fig. 4, E and F) suggests a distinct population of TAU with a different structural organization. CSA analysis of rpAD cases revealed a more complex pattern of protease-sensitive TAU profiles, with low or absent conformers unfolding at 2.75 M ($P < 0.001$) and 3.25 M Gdn HCl ($P = 0.002$) when compared to spAD cases (Fig. 7, E and F), and the patterns obtained with protease-sensitive 3R TAU were identical (fig. S5, E and F).

Conformational analysis of TAU forming TAU particles of different sizes

To investigate the conformational heterogeneity of TAU suggested by CSA deconvolution, we performed direct conformational analyses of TAU particles with different sizes that were obtained by fractionation of brain homogenates of individual AD cases by high-speed centrifugation in sucrose gradient (Fig. 8, A and B) and analyzed the conformation with CSA (Fig. 8, C to F) in fractions 1, 2, 3, and 4. The distinct CSA patterns in each fraction indicate that particles of different sizes have different conformational signatures and stability profiles, which compose the variable conformational profile of total insoluble TAU in the brain homogenate (Fig. 8, C to F). The experiments showed notable differences in the concentration of denaturant midpoint of unfolding (C_m) between fractions 2, 3, and 4 (Fig. 8G).

Next, we performed limited trypsin digestion of TAU in each fraction at constant TAU input and 1:10 trypsin/total protein ratio (Fig. 8H). The repeat core-specific mAb A16040D (epitope 269 to 281) produced signature profiles with a reproducible constant band at 24 kDa and ~37- and ~14-kDa bands with variable mass, different proportions after densitometry, and some additional weaker bands. As expected, the repeat core of TAU monomers floating on top of sucrose gradient (fraction 10) was completely digested by trypsin and did not generate any peptide pattern. Together, the presence of different trypsin profiles in different sucrose gradient fractions confirm the presence of misfolded TAU in each, with microtubule binding repeats protected from trypsin digestion. To investigate the relative proportion or different TAU fragments generated by trypsin in various sucrose fractions, we recorded the integrated peak density of each major band in Western blots. The data indicate significantly ($P < 0.05$) different profiles of fractions 4 and 1 in all six AD cases (Fig. 8I). These differential peptide patterns together with CDI and CSA profiles indicate that misfolded TAU particles with different masses and sedimentation velocities have distinct conformations.

DISCUSSION

Two aspects in late-onset AD that cannot be explained by genetic polymorphisms are (i) discrepancies between Aβ and TAU deposit burden and clinical disease severity (68) and (ii) the extensive variability of progression rates and phenotypes (12). Early seminal observations reporting different patterns of TAU aggregates in HEK reporter cells induced by TAU isolated from distinct tauopathies (15) and more recent studies with different TAU strains generated from monomers without seeds (69, 70) opened the possibility that alternatively structured TAU can encipher the information essential for distinct phenotypes observed in cells in vitro. Using recent biophysical techniques (41) to inventory the structural organization of TAU in the hippocampus, we have defined a potential variable in AD pathogenesis, namely, a cloud of misfolded TAU particles that have distinct structural organization and, in turn, different seeding potency. Our data demonstrate that different rates of cognitive decline in AD are associated with distinct TAU conformers and that clouds of misfolded 4R TAU conformers with high seeding potency might drive this process. The link to disease duration did not arise from the amount of TAU aggregates per se but from their distinct conformations. Further supporting this interpretation, each TAU isolate, here defined

operationally by deriving from an individual AD case, is rarely a singular conformational entity but typically a mixture of up to three different conformers that together give rise to distinct rpAD or spAD (fig. S6).

The conformational heterogeneity of brain TAU that we uncovered in sporadic AD implies the presence of numerous distinct structures that have very different propagation rates, interactomes, and toxicity and are associated with variable pathogenesis of AD. Although disease-causing mutations in the Aβ precursor protein and genes encoding its endoproteases have indisputably established the central role of Aβ in the pathogenesis of early-onset AD, the loose correlations between amyloid plaque load and severity of sporadic AD (68) and the failure of therapeutic interventions targeting misfolded Aβ have now generated a conundrum (12, 71). However, the second invariable marker of AD, the deposits of TAU aggregates, provide a more reliable indicator of cognitive decline, and the structural plasticity of recombinant TAU proteins observed in vitro suggests the need to improve our understanding of TAU structure in AD brain tissue.

On the basis of expression of all six TAU isoforms in an adult human brain, it has been assumed that all six are forming neurofibrillary tangles and that isoforms are probably randomly integrated into PHFs and straight filaments in AD (72–75). Our sedimentation velocity separation by high-speed centrifugation in sucrose gradient shows that misfolded TAU aggregates are, regardless of size, uniformly composed of ~80% of 4R TAU and ~20% of 3R TAU, although the soluble normal TAU monomers are mixtures of about equal proportions of 3R and 4R isoforms. The fourfold excess of 4R TAU in misfolded TAU aggregates indicates that unfolded 4R TAU monomers have higher propensity to conformational transition to β sheet structures in AD, and experiments with recombinant K18 and K19 substrates suggest that the mechanism is likely kinetic with faster conversion and growth of 4R aggregates. Thus far, we do not know whether aggregates represent distinct particles composed of only 4R or 3R TAU or whether both isoforms can contribute to make mixed particles. The recent cryo–electron microscopy (cryo-EM) models of core PHFs extracted from AD brains may accommodate upstream of V306 an additional 16 amino acids, which could represent a mixture of residues 259 to 274 (R1) from 3R TAU or 290 to 305 (R2) from 4R TAU (74, 75). It is notable that monitoring conformation of 3R TAU in misfolded aggregates generated nearly identical CDI and CSA conformational profiles to characteristics to total (3R + 4R) TAU, but assessing the single mixed particle versus distinct particle model will require high-resolution techniques such as immune(cryo)EM and measuring hydrogen exchange by mass spectrometry (HX MS).

Instead of the expected singular unique conformer of 4R tau linked to the rpAD phenotype, we found evidence of a cloud of misfolded conformers composed of up to three distinct populations of tau with varying structural organization and variable proportions in individual AD cases (fig. S6). This conformational model is supported by distinct sedimentation profiles of TAU aggregates, trypsin peptide maps, CDI, and CSA. Moreover, the CDI data indicate that differences in D/N ratio are due to the less exposed epitopes in the native conformation of TAU in rpAD and argue against substantial contribution of covalent cross-linking. Adding another layer to the conformational complexity are extensive posttranslational modifications of TAU, and using mass spectrometry, several papers

recently reported the differences in profiles of posttranslational modifications of insoluble tau that correlated with seeding potency of insoluble tau in different clinical phenotypes of late-onset AD (76, 77). Corresponding trends were also observed in early age of onset in familial AD with pesenilin-1 mutations (78). These and our direct conformational data presented here imply an interplay between post-translational modification and structural organization of TAU during AD development that warrants further investigation. Whether the differences in conformations are driving distinct posttranslational modifications or vice versa are important questions not only in AD but also in other tauopathies, including progressive supranuclear palsy, frontotemporal dementia, and Pick's disease. To address this question will require tools allowing simultaneous investigation of both and integrate cryo-EM for TAU filaments (fibrils) with conformation-sensitive mass spectrometry of TAU, such as HX MS or synchrotron footprinting that are applicable to both filamentous and oligomeric structures (28, 42, 57, 79). These approaches should also answer the question of whether the sedimentation velocity and different trypsin peptide patterns of TAU fractions in sucrose gradient are solely a result of conformation and particle size or are modified by posttranslational modifications, sarkosyl-resistant ligands, or attached lipids.

The protease sensitivity and lower stability of some of the misfolded TAU structures suggest that a substantial fraction of misfolded TAU is in an oligomeric state. Prior studies on yeast and rodent-adapted prions posit that lower stability of prion oligomers correlates with easier fragmentation, which is presumably responsible for faster replication and more rapid progression of disease (80, 81). However, examination of some rodent-adapted prions and most of human prions has revealed that this concept is not universally applicable; for example, a high affinity of strain-specific prion conformers for their substrate (the cellular prion protein) results in faster replication and propagation of more stable and protease-resistant prions (28, 42). Because our biophysical data indicate that a conformational cloud of more protease and Gdn HCl–resistant TAU is linked to faster replication in vitro, the hypothesis of TAU strain–specific, affinity-driven replication yields a better explanation for rapid progression in AD. There is an ongoing debate whether, and which of, the oligomers of TAU observed in in vitro experimental paradigms exist in the brains of patients with AD and what role they play in AD pathogenesis (12). Our experiments provide direct evidence for a broad spectrum of TAU conformers in AD brains, which group into three major peaks in CSA. Thus far, we have not yet identified whether these differences are due to the structure of the monomeric building block or the way the monomers are assembled (quaternary fibril structure), but the prevailing view is that both of these aspects must be thermodynamically and kinetically related (82). Whether different slopes of replication that we observed in seeding experiments are indicative of distinct mechanisms such as theoretically proposed TAU fibril growth from ends or from sites (83) will require further investigation using electron or atomic force microscopy. Recent evidence from human and animal prion strains also indicate that nonprotein cofactors such as negatively charged polyanions, gangliosides, and phospholipids might play a critical role in particular strain stability and propagation (28, 57, 84–86). Whether such auxiliary cofactors exist in TAU strains is a critical next question, which may improve our understanding of differential interactomes, propagation rates, and targeting of distinct host cells by specific TAU strains.

Together with our recent report on conformational evolution of TAU strains in FTLD caused by a MAPT P301L mutation (41), the biophysical data demonstrate extensive conformational range of distinct TAU strains that are associated with different phenotypes of disease and rates of clinical decline in AD as well. Moreover, the findings of different strains of Aβ that parallel distinct cloud of TAU conformers in rpAD (9, 10) suggest a pathogenetic association and imply a dual prion-like synergy, as recently proposed from studies in vitro (87). In addition, the polymorphisms of *APOE* gene in AD cases and distinct TAU strains suggest a potential parallel to a situation noted for human prions, where the interplay between common polymorphisms in the prion protein gene (*PRNP*) and variable conformational characteristics of the pathogenic prion protein leads to vastly different disease clinicopathological outcomes (45–47). Our findings might help the development of individual-based diagnostics and molecular classification of AD subtypes, which are prerequisites for AD therapeutic strategies that will need to consider clouds of conformers with extensive interindividual variability.

MATERIALS AND METHODS

Study design

The aim of this study was to investigate structural organization and replication potency of misfolded aggregates of TAU protein present in the hippocampus of patients with different progression rates of AD. The concentration and conformational characteristics of TAU protein isoforms were determined in three independent experiments using biophysical methods based on our previous work (9, 28, 34, 41). The sample size for biophysical and time points for cell experiments were chosen on the basis of data reported earlier (41, 88) to obtain a significant difference for the expected variability. Deidentified, randomly assigned, and gender-balanced human postmortem brain tissue samples were collected from brain bank repositories located at CWRU (table S1). The identity of the samples was replaced with an internal code, and the investigators performing the experiments were blinded to the sample identity during testing and analysis. Experimental replicates for each experiment are listed in the figure legends.

Statistical analysis

Cumulative survival curves were constructed by the Kaplan-Meier method, both overall and by stratifying for each of the above variables. Comparisons of survival curves among groups were carried out by the log-rank (Mantel-Cox) test. We investigated the effect of concentration and stability of pathogenic TAU strains in Gdn HCl before and after PK treatment (34, 41, 98) on clinicopathological phenotype and duration of the disease in AD cases. In the comparisons of different groups, *P* values at given Gdn HCl concentration in CSA were calculated using analysis of variance (ANOVA) and two-tailed Fisher's exact test, and unfolding curves of TAU among different clinical phenotypes of AD cases were compared by the two-tailed log-rank (Mantel-Cox) and two-tailed generalized Wilcoxon test. The two-sided power analysis to determine the sample size impact and all other statistical analyses including regression modeling were performed using SPSS 27 software (Statistical Package for Social Sciences, SPSS Inc.).

Supplementary Material

Refer to Web version on PubMed Central for supplementary material.

Acknowledgments:

We are grateful to the patients' families, the CJD Foundation, referring physicians, and all the members of the CWRU Alzheimer's Disease Center and National Prion Disease Pathology Surveillance Center for technical help and review of data. We are indebted to E. Gelpi, S. Borrego-Ecija, L. Molina-Porcel, and T. Ximelis of the Neurological Tissue Bank of the Biobank-Hospital Clinic-IDIBAPS, Barcelona, Spain for FTLD MAPT P301L and Pick's disease sample and data procurement and to all brain donors and their families for brain donation for research. We are grateful to A. Miron for Illumina and Sanger sequencing, W. Surewicz for K18 and K19 plasmids, and E. Poptic for scaled-up production of RD3 antibody.

Funding:

Work in the Safar laboratory was supported by grants from BrightFocus Foundation (A2016085S), Alberta Innovates Biosolutions (FP00209618), and NIH (1RF1AG058267 and 1RF1AG061797). Westaway laboratory was funded by a Canada Research Chair (tier 1), CIHR (PS148962 and GER 163048), and Alberta Innovates Biosolutions (ABIBS AEP 201600021 and 20160023). The NACC database is funded by NIA grant U01 AG016976.

Data and materials availability:

All data associated with this study are present in the paper or the Supplementary Materials.

REFERENCES AND NOTES

1. Jun G, Ibrahim-Verbaas CA, Vronskaya M et al. A novel Alzheimer disease locus located near the gene encoding TAU protein. Mol. Psychiatry 21, 108–117 (2016). [PubMed: 25778476]
2. Kunkle BW, Grenier-Boley B, Sims R et al. Genetic meta-analysis of diagnosed Alzheimer's disease identifies new risk loci and implicates Aβ, TAU, immunity and lipid processing. Nat. Genet 51, 414–430 (2019). [PubMed: 30820047]
3. Chitravas N, Jung RS, Kofskey DM, Blevins JE, Gambetti P, Leigh RJ, Cohen ML, Treatable neurological disorders misdiagnosed as Creutzfeldt-Jakob disease. Ann. Neurol 70, 437–444 (2011). [PubMed: 21674591]
4. Schmidt C, Wolff M, Weitz M, Bartlau T, Korth C, Zerr I, Rapidly progressive Alzheimer disease. Arch. Neurol 68, 1124–1130 (2011). [PubMed: 21911694]
5. Schmidt C, Redyk K, Meissner B, Krack L, von Ahsen N, Roeber S, Kretzschmar H, Zerr I, Clinical features of rapidly progressive Alzheimer's disease. Dement. Geriatr. Cogn. Disord 29, 371–378 (2020).
6. Schmidt C, Artjomova S, Hoeschel M, Zerr I, CSF prion protein concentration and cognition in patients with Alzheimer disease. Prion 7, 229–234 (2013) [PubMed: 23406922]
7. Schmidt C, Haik S, Satoh K, Rabano A, Martinez-Martin P, Roeber S, Brandel JP, Calero-Lara M, de Pedro-Cuesta J, Laplanche JL, Hauw JJ, Kretzschmar H, Zerr I, Rapidly progressive Alzheimer's disease: A multicenter update. J. Alzheimers Dis 30, 751–756 (2012). [PubMed: 22460329]
8. Pillai JA, Appleby BS, Safar J, Leverenz JB, Rapidly progressive Alzheimer's disease in two distinct autopsy cohorts. J. Alzheimers Dis 64, 973–980 (2018). [PubMed: 29966195]
9. Cohen ML, Kim C, Haldiman T, ElHag M, Mehndiratta P, Pichet T, Lissemore F, Shea M, Cohen Y, Chen W, Blevins J, Appleby BS, Surewicz K, Surewicz WK, Sajatovic M, Tatsuoka C, Zhang S, Mayo P, Butkiewicz M, Haines JL, Lerner AJ, Safar JG, Rapidly progressive Alzheimer's disease features distinct structures of amyloid-β. Brain 138, 1009–1022 (2015). [PubMed: 25688081]
10. Qiang W, Yau WM, Lu JX, Collinge J, Tycko R, Structural variation in amyloid-β fibrils from Alzheimer's disease clinical subtypes. Nature 541, 217–221 (2017). [PubMed: 28052060]
11. Drummond E, Nayak S, Faustin A, Pires G, Hickman RA, Askenazi M, Cohen M, Haldiman T, Kim C, Han X, Shao Y, Safar JG, Ueberheide B, Wisniewski T, Proteomic differences in amyloid

plaques in rapidly progressive and sporadic Alzheimer's disease. Acta Neuropathol. 133, 933–954 (2017). [PubMed: 28258398]

12. Gallardo G, Holtzman DM, Amyloid-β and Tau at the crossroads of Alzheimer's disease. Adv. Exp. Med. Biol 1184, 187 (2019). [PubMed: 32096039]
13. Braak H, Del Tredici K, Evolutional aspects of Alzheimer's disease pathogenesis. J. Alzheimers Dis 33 (Suppl. 1), S155–S161 (2013). [PubMed: 22699850]
14. Kaufman SK, Del Tredici K, Thomas TL, Braak H, Diamond MI, Tau seeding activity begins in the transentorhinal/entorhinal regions and anticipates phospho-TAU pathology in Alzheimer's disease and PART. Acta Neuropathol. 136, 57–67 (2018). [PubMed: 29752551]
15. Sanders DW, Kaufman SK, Holmes BB, Diamond MI, Prions and protein assemblies that convey biological information in health and disease. Neuron 89, 433–448 (2016). [PubMed: 26844828]
16. Caughey B, Baron GS, Chesebro B, Jeffrey M, Getting a grip on prions: Oligomers, amyloids, and pathological membrane interactions. Annu. Rev. Biochem 78, 177–204 (2009). [PubMed: 19231987]
17. Cobb NJ, Surewicz WK, Prion diseases and their biochemical mechanisms. Biochemistry 48, 2574–2585 (2009). [PubMed: 19239250]
18. Morales R, Abid K, Soto C, The prion strain phenomenon: Molecular basis and unprecedented features. Biochim. Biophys. Acta 1772, 681–691 (2007). [PubMed: 17254754]
19. Prusiner SB, in Principles of Molecular Medicine, Jameson JL, Ed. (Humana Press, 1998), pp. 927–939.
20. Prusiner SB, Legname G, DeArmond SJ, Cohen FE, Safar J, Riesner D, Kaneko K, in Prion Biology and Diseases, Prusiner SB, Ed. (Cold Spring Harbor Laboratory Press, 2004), pp. 857–920.
21. Barria MA, Mukherjee A, Gonzalez-Romero D, Morales R, Soto C, De novo generation of infectious prions in vitro produces a new disease phenotype. PLOS Pathog. 5, e1000421 (2009). [PubMed: 19436715]
22. Castilla J, Saa P, Hetz C, Soto C, *In vitro* generation of infectious scrapie prions. Cell 121, 195–206 (2005, 2005). [PubMed: 15851027]
23. Deleault NR, Harris BT, Rees JR, Supattapone S, Formation of native prions from minimal components in vitro. Proc. Natl. Acad. Sci. U.S.A 104, 9741–9746 (2007). [PubMed: 17535913]
24. Geoghegan JC, Miller MB, Kwak AH, Harris BT, Supattapone S, Trans-dominant inhibition of prion propagation in vitro is not mediated by an accessory cofactor. PLOS Pathog. 5, e1000535 (2009). [PubMed: 19649330]
25. Kim JI, Cali I, Surewicz K, Kong Q, Raymond GJ, Atarashi R, Race B, Qing L, Gambetti P, Caughey B, Surewicz WK, Mammalian prions generated from bacterially expressed prion protein in the absence of any mammalian cofactors. J. Biol. Chem 285, 14083–14087 (2010). [PubMed: 20304915]
26. Legname G, Baskakov IV, Nguyen H-OB, Riesner D, Cohen FE, DeArmond SJ, Prusiner SB, Synthetic mammalian prions. Science 305, 673–676 (2004). [PubMed: 15286374]
27. Wang F, Wang X, Yuan CG, Ma J, Generating a prion with bacterially expressed recombinant prion protein. Science 327, 1132–1135 (2010). [PubMed: 20110469]
28. Kim C, Xiao X, Chen S, Haldiman T, Smirnovas V, Kofskey D, Warren M, Surewicz K, Maurer NR, Kong Q, Surewicz W, Safar JG, Artificial strain of human prions created in vitro. Nat. Commun 9, 2166 (2018). [PubMed: 29867164]
29. Wickner RB, [URE3] as an altered URE2 protein: Evidence for a prion analog in *Saccharomyces cerevisiae*. Science 264, 566–569 (1994). [PubMed: 7909170]
30. Glover JR, Kowal AS, Schirmer EC, Patino MM, Liu J-J, Lindquist S, Self-seeded fibers formed by Sup35, the protein determinant of [*PSI*$^{+}$], a heritable prion-like factor of *S. cerevisiae*. Cell 89, 811–819 (1997). [PubMed: 9182769]
31. Kabir ME, Safar JG, Implications of prion adaptation and evolution paradigm for human neurodegenerative diseases. Prion 8, 111–116 (2014). [PubMed: 24401672]
32. Kim C, Haldiman T, Surewicz K, Cohen Y, Chen W, Blevins J, Sy MS, Cohen M, Kong Q, Telling GC, Surewicz WK, Safar JG, Small protease sensitive oligomers of PrPSc in distinct human prions determine conversion rate of PrPC. PLOS Pathog. 8, e1002835 (2012). [PubMed: 22876179]

33. Kim C, Haldiman T, Cohen Y, Chen W, Blevins J, Sy MS, Cohen M, Safar JG, Protease-sensitive conformers in broad spectrum of distinct PrPSc structures in sporadic Creutzfeldt-Jakob disease are indicator of progression rate. PLOS Pathog. 7, e1002242 (2011). [PubMed: 21931554]
34. Safar J, Wille H, Itri V, Groth D, Serban H, Torchia M, Cohen FE, Prusiner SB, Eight prion strains have PrP^{Sc} molecules with different conformations. Nat. Med 4, 1157–1165 (1998). [PubMed: 9771749]
35. Montine TJ, Phelps CH, Beach TG, Bigio EH, Cairns NJ, Dickson DW, Duyckaerts C, Frosch MP, Masliah E, Mirra SS, Nelson PT, Schneider JA, Thal DR, Trojanowski JQ, Vinters HV, Hyman BT; National Institute on Aging; Alzheimer's Association, National Institute on Aging-Alzheimer's Association guidelines for the neuropathologic assessment of Alzheimer's disease: A practical approach. Acta Neuropathol. 123, 1–11 (2012). [PubMed: 22101365]
36. Geschwind MD, Shu H, Haman A, Sejvar JJ, Miller BL, Rapidly progressive dementia. Ann. Neurol 64, 97–108 (2008). [PubMed: 18668637]
37. Pillai JA, Bonner-Jackson A, Bekris LM, Safar J, Bena J, Leverenz JB, Highly elevated cerebrospinal fluid total Tau level reflects higher likelihood of non-amnestic subtype of Alzheimer's disease. J. Alzheimers Dis 70, 1051–1058 (2019). [PubMed: 31306137]
38. Schmidt C, Karch A, Artjomova S, Hoeschel M, Zerr I, Pre-progression rates in Alzheimer's disease revisited. J. Alzheimers Dis 35, 451–454 (2013). [PubMed: 23435410]
39. Schmidt C, Wolff M, von Ahsen N, Zerr I, Alzheimer's disease: Genetic polymorphisms and rate of decline. Dement. Geriatr. Cogn. Disord 33, 84–89 (2012). [PubMed: 22414550]
40. Cohen M, Appleby B, Safar JG, Distinct prion-like strains of amyloid beta implicated in phenotypic diversity of Alzheimer's disease. Prion 10, 9–17 (2016). [PubMed: 26809345]
41. Daude N, Kim C, Kang SG, Eskandari-Sedighi G, Haldiman T, Yang J, Fleck SC, Gomez-Cardona E, Han ZZ, Borrego-Ecija S, Wohlgemuth S, Julien O, Wille H, Molina-Porcel L, Gelpi E, Safar JG, Westaway D, Diverse, evolving conformer populations drive distinct phenotypes in frontotemporal lobar degeneration caused by the same MAPT-P301L mutation. Acta Neuropathol. 139, 1045–1070 (2020). [PubMed: 32219515]
42. Safar JG, Xiao X, Kabir ME, Chen S, Kim C, Haldiman T, Cohen Y, Chen W, Cohen ML, Surewicz WK, Structural determinants of phenotypic diversity and replication rate of human prions. PLOS Pathog. 11, e1004832 (2015). [PubMed: 25875953]
43. Haldiman T, Kim C, Cohen Y, Chen W, Blevins J, Qing L, Cohen ML, Langeveld J, Telling GC, Kong Q, Safar JG, Co-existence of distinct prion types enables conformational evolution of human PrPSc by competitive selection. J. Biol. Chem 288, 29846–29861 (2013). [PubMed: 23974118]
44. Atarashi R, Moore RA, Sim VL, Hughson AG, Dorward DW, Onwubiko HA, Priola SA, Caughey B, Ultrasensitive detection of scrapie prion protein using seeded conversion of recombinant prion protein. Nat. Methods 4, 645–650 (2007). [PubMed: 17643109]
45. Puoti G, Bizzi A, Forloni G, Safar JG, Tagliavini F, Gambetti P, Sporadic human prion diseases: Molecular insights and diagnosis. Lancet Neurol. 11, 618–628 (2012). [PubMed: 22710755]
46. Safar JG, in Prions and Diseases, Zou W-Q, Gambetti P, Ed. (Springer Verlag, 2012), vol. 1.
47. Safar JG, Molecular pathogenesis of sporadic prion diseases in man. Prion 6, 108–115 (2012). [PubMed: 22421210]
48. Minjarez B, Valero Rustarazo ML, Sanchez del Pino MM, González-Robles A, Sosa-Melgarejo JA, Luna-Muñoz J, Mena R, Luna-Arias JP, Identification of polypeptides in neurofibrillary tangles and total homogenates of brains with Alzheimer's disease by tandem mass spectrometry. J. Alzheimers Dis 34, 239–262 (2013). [PubMed: 23229080]
49. Buée L, Troquier L, Burnouf S, Belarbi K, Van der Jeugd A, Ahmed T, Fernandez-Gomez F, Caillierez R, Grosjean ME, Begard S, Barbot B, Demeyer D, Obriot H, Brion I, Buée-Scherrer V, Maurage CA, Balschun D, D'Hooge R, Hamdane M, Blum D, Sergeant N, From TAU phosphorylation to TAU aggregation: What about neuronal death? Biochem. Soc. Trans 38, 967–972 (2010). [PubMed: 20658986]
50. Stoothoff WH, Johnson GV, Tau phosphorylation: Physiological and pathological consequences. Biochim. Biophys. Acta 1739, 280–297 (2005). [PubMed: 15615646]

51. Irwin DJ, Cohen TJ, Grossman M, Arnold SE, McCarty-Wood E, Van Deerlin VM, Lee VM, Trojanowski JQ, Acetylated TAU neuropathology in sporadic and hereditary TAUopathies. Am. J. Pathol 183, 344–351 (2013). [PubMed: 23885714]
52. Min SW, Chen X, Tracy TE, Li Y, Zhou Y, Wang C, Shirakawa K, Minami SS, Defensor E, Mok SA, Sohn PD, Schilling B, Cong X, Ellerby L, Gibson BW, Johnson J, Krogan N, Shamloo M, Gestwicki J, Masliah E, Verdin E, Gan L, Critical role of acetylation in TAU-mediated neurodegeneration and cognitive deficits. Nat. Med 21, 1154–1162 (2015). [PubMed: 26390242]
53. Park S, Lee JH, Jeon JH, Lee MJ, Degradation or aggregation: The ramifications of post-translational modifications on TAU. BMB Rep. 51, 265–273 (2018). [PubMed: 29661268]
54. Kovacs GG, Molecular pathology of neurodegenerative diseases: Principles and practice. J. Clin. Pathol 72, 725–735 (2019). [PubMed: 31395625]
55. Mays CE, van der Merwe J, Kim C, Haldiman T, McKenzie D, Safar JG, Westaway D, Prion infectivity plateaus and conversion to symptomatic disease originate from falling precursor levels and increased levels of oligomeric PrPSc species. J. Virol 89, 12418–12426 (2015). [PubMed: 26423957]
56. Jeganathan S, von Bergen M, Brutlach H, Steinhoff HJ, Mandelkow E, Global hairpin folding of TAU in solution. Biochemistry 45, 2283–2293 (2006). [PubMed: 16475817]
57. Li Q, Wang F, Xiao X, Kim C, Bohon J, Kiselar J, Safar JG, Ma J, Surewicz WK, Structural attributes of mammalian prion infectivity: Insights from studies with synthetic prions. J. Biol. Chem 293, 18494–18503 (2018). [PubMed: 30275016]
58. Groveman BR, Orru CD, Hughson AG, Raymond LD, Zanusso G, Ghetti B, Campbell KJ, Safar J, Galasko D, Caughey B, Rapid and ultra-sensitive quantitation of disease-associated α-synuclein seeds in brain and cerebrospinal fluid by αSyn RT-QuIC. Acta Neuropathol. Commun 6, 7 (2018). [PubMed: 29422107]
59. Foutz A, Appleby BS, Hamlin C, Liu X, Yang S, Cohen Y, Chen W, Blevins J, Fausett C, Wang H, Gambetti P, Zhang S, Hughson A, Tatsuoka C, Schonberger LB, Cohen ML, Caughey B, Safar JG, Diagnostic and prognostic value of human prion detection in cerebrospinal fluid. Ann. Neurol 81, 79–92 (2017). [PubMed: 27893164]
60. Jeganathan S, von Bergen M, Mandelkow EM, Mandelkow E, The natively unfolded character of TAU and its aggregation to Alzheimer-like paired helical filaments. Biochemistry 47, 10526–10539 (2008). [PubMed: 18783251]
61. Daebel V, Chinnathambi S, Biernat J, Schwalbe M, Habenstein B, Loquet A, Akoury E, Tepper K, Muller H, Baldus M, Griesinger C, Zweckstetter M, Mandelkow E, Vijayan V, Lange A, β-Sheet core of tau paired helical filaments revealed by solid-state NMR. J. Am. Chem. Soc 134, 13982 (2012). [PubMed: 22862303]
62. Taniguchi-Watanabe S, Arai T, Kametani F, Nonaka T, Masuda-Suzukake M, Tarutani A, Murayama S, Saito Y, Arima K, Yoshida M, Akiyama H, Robinson A, Mann DMA, Iwatsubo T, Hasegawa M, Biochemical classification of TAUopathies by immunoblot, protein sequence and mass spectrometric analyses of sarkosyl-insoluble and trypsin-resistant TAU. Acta Neuropathol. 131, 267–280 (2016). [PubMed: 26538150]
63. Orru CD, Wilham JM, Vascellari S, Hughson AG, Caughey B, New generation QuIC assays for prion seeding activity. Prion 6, 147–152 (2012). [PubMed: 22421206]
64. Oelschlegel AM, Weissmann C, Acquisition of drug resistance and dependence by prions. PLOS Pathog. 9, e1003158 (2013). [PubMed: 23408888]
65. Li J, Browning S, Mahal SP, Oelschlegel AM, Weissmann C, Darwinian evolution of prions in cell culture. Science 327, 869–872 (2010). [PubMed: 20044542]
66. Safarian S, Alimohammadi M, Saberi AA, Moosavi-Movahedi AA, A statistical mechanical deconvolution of the differential scanning calorimetric profiles of the thermal denaturation of cyanomethemoglobin. Protein J. 24, 175–181 (2005). [PubMed: 16096723]
67. Azuaga AI, Dobson CM, Mateo PL, Conejero-Lara F, Unfolding and aggregation during the thermal denaturation of streptokinase. Eur. J. Biochem 269, 4121–4133 (2002). [PubMed: 12180989]
68. Masters CL, Selkoe DJ, Biochemistry of amyloid β-protein and amyloid deposits in Alzheimer disease. Cold Spring Harb. Perspect. Med 2, a006262 (2012). [PubMed: 22675658]

69. Mirbaha H, Chen D, Morazova OA, Ruff KM, Sharma AM, Liu X, Goodarzi M, Pappu RV, Colby DW, Mirzaei H, Joachimiak LA, Diamond MI, Inert and seed-competent TAU monomers suggest structural origins of aggregation. eLife 7, e36584 (2018). [PubMed: 29988016]
70. Sharma AM, Thomas TL, Woodard DR, Kashmer OM, Diamond MI, Tau monomer encodes strains. eLife 7, e37813 (2018). [PubMed: 30526844]
71. Cummings J, Lee G, Ritter A, Sabbagh M, Zhong K, Alzheimer's disease drug development pipeline: 2019. Alzheimers Dement. 5, 272–293 (2019).
72. Zhang W, Falcon B, Murzin AG, Fan J, Crowther RA, Goedert M, Scheres SHW, Heparin-induced tau filaments are polymorphic and differ from those in Alzheimer's and Pick's diseases. eLife 8, e43584 (2019). [PubMed: 30720432]
73. Falcon B, Zivanov J, Zhang W, Murzin AG, Garringer HJ, Vidal R, Crowther RA, Newell KL, Ghetti B, Goedert M, Scheres SHW, Novel tau filament fold in chronic traumatic encephalopathy encloses hydrophobic molecules. Nature 568, 420–423 (2019). [PubMed: 30894745]
74. Goedert M, Tau filaments in neurodegenerative diseases. FEBS Lett. 592, 2383–2391 (2018). [PubMed: 29790176]
75. Falcon B, Zhang W, Schweighauser M, Murzin AG, Vidal R, Garringer HJ, Ghetti B, Scheres SHW, Goedert M, Tau filaments from multiple cases of sporadic and inherited Alzheimer's disease adopt a common fold. Acta Neuropathol. 136, 699–708 (2018). [PubMed: 30276465]
76. Wesseling H, Mair W, Kumar M, Schlaffner CN, Tang S, Beerepoot P, Fatou B, Guise AJ, Cheng L, Takeda S, Muntel J, Rotunno MS, Dujardin S, Davies P, Kosik KS, Miller BL, Berretta S, Hedreen JC, Grinberg LT, Seeley WW, Hyman BT, Steen H, Steen JA, Tau PTM profiles identify patient heterogeneity and stages of Alzheimer's disease. Cell 183, 1699–1713.e13 (2020). [PubMed: 33188775]
77. Dujardin S, Commins C, Lathuiliere A, Beerepoot P, Fernandes AR, Kamath TV, De Los Santos MB, Klickstein N, Corjuc DL, Corjuc BT, Dooley PM, Viode A, Oakley DH, Moore BD, Mullin K, Jean-Gilles D, Clark R, Atchison K, Moore R, Chibnik LB, Tanzi RE, Frosch MP, Serrano-Pozo A, Elwood F, Steen JA, Kennedy ME, Hyman BT, Tau molecular diversity contributes to clinical heterogeneity in Alzheimer's disease. Nat. Med 26, 1256–1263 (2020). [PubMed: 32572268]
78. Sepulveda-Falla D, Chavez-Gutierrez L, Portelius E, Vélez JI, Dujardin S, Barrera-Ocampo A, Dinkel F, Hagel C, Puig B, Mastronardi C, Lopera F, Hyman BT, Blennow K, Arcos-Burgos M, de Strooper B, Glatzel M, A multifactorial model of pathology for age of onset heterogeneity in familial Alzheimer's disease. Acta Neuropathol. 141, 217–233 (2021). [PubMed: 33319314]
79. Siddiqi MK, Kim C, Haldiman T, Kacirova M, Wang B, Bohon J, Chance MR, Kiselar J, Safar JG, Structurally distinct external solvent-exposed domains drive replication of major human prions. PLOS Pathog. 17, e1009642 (2021). [PubMed: 34138981]
80. Legname G, Nguyen H-OB, Peretz D, Cohen FE, DeArmond SJ, Prusiner SB, Continuum of prion protein structures enciphers a multitude of prion isolate-specified phenotypes. Proc. Natl. Acad. Sci. U.S.A 103, 19105–19110 (2006). [PubMed: 17142317]
81. Tanaka M, Collins SR, Toyama BH, Weissman JS, The physical basis of how prion conformations determine strain phenotypes. Nature 442, 585–589 (2006). [PubMed: 16810177]
82. Paravastu AK, Leapman RD, Yau WM, Tycko R, Molecular structural basis for polymorphism in Alzheimer's beta-amyloid fibrils. Proc. Natl. Acad. Sci. U.S.A 105, 18349–18354 (2008). [PubMed: 19015532]
83. Michaels TCT, šarić A, Habchi J, Chia S, Meisl G, Vendruscolo M, Dobson CM, Knowles TPJ, Chemical kinetics for bridging molecular mechanisms and macroscopic measurements of amyloid fibril formation. Annu. Rev. Phys. Chem 69, 273–298 (2018). [PubMed: 29490200]
84. Noble GP, Wang DW, Walsh DJ, Barone JR, Miller MB, Nishina KA, Li S, Supattapone S, A structural and functional comparison between infectious and non-Infectious autocatalytic recombinant PrP conformers. PLOS Pathog. 11, e1005017 (2015). [PubMed: 26125623]
85. Deleault NR, Walsh DJ, Piro JR, Wang F, Wang X, Ma J, Rees JR, Supattapone S, Cofactor molecules maintain infectious conformation and restrict strain properties in purified prions. Proc. Natl. Acad. Sci. U.S.A 109, E1938–E1946 (2012). [PubMed: 22711839]

86. Deleault NR, Piro JR, Walsh DJ, Wang F, Ma J, Geoghegan JC, Supattapone S, Isolation of phosphatidylethanolamine as a solitary cofactor for prion formation in the absence of nucleic acids. Proc. Natl. Acad. Sci. U.S.A 109, 8546–8551 (2012). [PubMed: 22586108]

87. Aoyagi A, Condello C, Stöhr J, Yue W, Rivera BM, Lee JC, Woerman AL, Halliday G, van Duinen S, Ingelsson M, Lannfelt L, Graff C, Bird TD, Keene CD, Seeley WW, DeGrado WF, Prusiner SB, Aβ and tau prion-like activities decline with longevity in the Alzheimer's disease human brain. Sci. Transl. Med 11, eaat8462 (2019). [PubMed: 31043574]

88. Kang SG, Han ZZ, Daude N, McNamara E, Wohlgemuth S, Molina-Porcel L, Safar JG, Mok SA, Westaway D, Pathologic tau conformer ensembles induce dynamic, liquid-liquid phase separation events at the nuclear envelope. BMC Biol. 19, 199 (2021). [PubMed: 34503506]

89. Tatsuoka C, Tseng H, Jaeger J, Varadi F, Smith MA, Yamada T, Smyth KA, Lerner AJ; The Alzheimer's Disease Neuroimaging Initiative, Modeling the heterogeneity in risk of progression to Alzheimer's disease across cognitive profiles in mild cognitive impairment. Alzheimers Res. Ther 5, 14 (2013). [PubMed: 23497709]

90. Chien DT, Szardenings AK, Bahri S, Walsh JC, Mu F, Xia C, Shankle WR, Lerner AJ, Su MY, Elizarov A, Kolb HC, Early clinical PET imaging results with the novel PHF-tau radioligand [F18]-T808. J. Alzheimers Dis 38, 171–184 (2014). [PubMed: 23948934]

91. McKhann GM, Knopman DS, Chertkow H, Hyman BT, Jack CR Jr., Kawas CH, Klunk WE, Koroshetz WJ, Manly JJ, Mayeux R, Mohs RC, Morris JC, Rossor MN, Scheltens P, Carrillo MC, Thies B, Weintraub S, Phelps CH, The diagnosis of dementia due to Alzheimer's disease: Recommendations from the National Institute on Aging-Alzheimer's Association workgroups on diagnostic guidelines for Alzheimer's disease. Alzheimers Dement. 7, 263–269 (2011). [PubMed: 21514250]

92. Hyman BT, Phelps CH, Beach TG, Bigio EH, Cairns NJ, Carrillo MC, Dickson DW, Duyckaerts C, Frosch MP, Masliah E, Mirra SS, Nelson PT, Schneider JA, Thal DR, Thies B, Trojanowski JQ, Vinters HV, Montine TJ, National Institute on Aging-Alzheimer's Association guidelines for the neuropathologic assessment of Alzheimer's disease. Alzheimers Dement. 8, 1–13 (2012). [PubMed: 22265587]

93. Beekly DL, Ramos EM, Lee WW, Deitrich WD, Jacka ME, Wu J, Hubbard JL, Koepsell TD, Morris JC, Kukull WA; NIA Alzheimer's Disease Centers, The National Alzheimer's Coordinating Center (NACC) database: The Uniform Data Set. Alzheimer Dis. Assoc. Disord 21, 249–258 (2007). [PubMed: 17804958]

94. Parchi P, Zou W, Wang W, Brown P, Capellari S, Ghetti B, Kopp N, Schulz-Schaeffer WJ, Kretzschmar HA, Head MW, Ironside JW, Gambetti P, Chen SG, Genetic influence on the structural variations of the abnormal prion protein. Proc. Natl. Acad. Sci. U.S.A 97, 10168–10172 (2000). [PubMed: 10963679]

95. Safar JG, Geschwind MD, Deering C, Didorenko S, Sattavat M, Sanchez H, Serban A, Vey M, Baron H, Giles K, Miller BL, DeArmond SJ, Prusiner SB, Diagnosis of human prion disease. Proc. Natl. Acad. Sci. U.S.A 102, 3501–3501 (2005). [PubMed: 15741275]

96. Sanger F, Nicklen S, Coulson AR, DNA sequencing with chain-terminating inhibitors. Proc. Natl. Acad. Sci. U.S.A 74, 5463–5467 (1977). [PubMed: 271968]

97. Rascovsky K, Hodges JR, Knopman D, Mendez MF, Kramer JH, Neuhaus J, van Swieten JC, Seelaar H, Dopper EG, Onyike CU, Hillis AE, Josephs KA, Boeve BF, Kertesz A, Seeley WW, Rankin KP, Johnson JK, Gorno-Tempini ML, Rosen H, Prioleau-Latham CE, Lee A, Kipps CM, Lillo P, Piguet O, Rohrer JD, Rossor MN, Warren JD, Fox NC, Galasko D, Salmon DP, Black SE, Mesulam M, Weintraub S, Dickerson BC, Diehl-Schmid J, Pasquier F, Deramecourt V, Lebert F, Pijnenburg Y, Chow TW, Manes F, Grafman J, Cappa SF, Freedman M, Grossman M, Miller BL, Sensitivity of revised diagnostic criteria for the behavioural variant of frontotemporal dementia. Brain 134, 2456–2477 (2011). [PubMed: 21810890]

98. Safar J, Prusiner SB, Chapter 29 Molecular studies of prion diseases. Prog. Brain Res 117 421–434 (1998). [PubMed: 9932423]

99. de Silva R, Lashley T, Gibb G, Hanger D, Hope A, Reid A, Bandopadhyay R, Utton M, Strand C, Jowett T, Khan N, Anderton B, Wood N, Holton J, Revesz T, Lees A, Pathological inclusion bodies in TAUopathies contain distinct complements of TAU with three or four microtubule-

binding repeat domains as demonstrated by new specific monoclonal antibodies. Neuropathol. Appl. Neurobiol 29, 288–302 (2003). [PubMed: 12787326]

100. Luk KC, Song C, O'Brien P, Stieber A, Branch JR, Brunden KR, Trojanowski JQ, Lee VM, Exogenous alpha-synuclein fibrils seed the formation of Lewy body-like intracellular inclusions in cultured cells. Proc. Natl. Acad. Sci. U.S.A 106, 20051–20056 (2009). [PubMed: 19892735]
101. Safar JG, DeArmond SJ, Kociuba K, Deering C, Didorenko S, Bouzamondo-Bernstein E, Prusiner SB, Tremblay P, Prion clearance in bigenic mice. J. Gen. Virol 86, 2913–2923 (2005). [PubMed: 16186247]
102. Safar JG, Kellings K, Serban A, Groth D, Cleaver JE, Prusiner SB, Riesner D, Search for a prion-specific nucleic acid. J. Virol 79, 10796–10806 (2005). [PubMed: 16051871]
103. Dinkel PD, Siddiqua A, Huynh H, Shah M, Margittai M, Variations in filament conformation dictate seeding barrier between three- and four-repeat TAU. Biochemistry 50, 4330–4336 (2011). [PubMed: 21510682]
104. Lee IS, Long JR, Prusiner SB, Safar JG, Selective precipitation of prions by polyoxometalate complexes. J. Am. Chem. Soc 127, 13802–13803 (2005). [PubMed: 16201796]
105. Safar JG, Wille H, Geschwind MD, Deering C, Latawiec D, Serban A, King DJ, Legname G, Weisgraber KH, Mahley RW, Miller BL, DeArmond SJ, Prusiner SB, Human prions and plasma lipoproteins. Proc. Natl. Acad. Sci. U.S.A 103, 11312–11317 (2006). [PubMed: 16849426]
106. Safar JG, Scott M, Monaghan J, Deering C, Didorenko S, Vergara J, Ball H, Legname G, Leclerc E, Solforosi L, Serban H, Groth D, Burton DR, Prusiner SB, Williamson RA, Measuring prions causing bovine spongiform encephalopathy or chronic wasting disease by immunoassays and transgenic mice. Nat. Biotechnol 20, 1147–1150 (2002). [PubMed: 12389035]
107. Mays CE, Kim C, Haldiman T, van der Merwe J, Lau A, Yang J, Grams J, Di Bari MA, Nonno R, Telling GC, Kong Q, Langeveld J, McKenzie D, Westaway D, Safar JG, Prion disease tempo determined by host-dependent substrate reduction. J. Clin. Invest 124, 847–858 (2014). [PubMed: 24430187]
108. Prusiner SB, Hadlow WJ, Eklund CM, Race RE, Cochran SP, Sedimentation characteristics of the scrapie agent from murine spleen and brain. Biochemistry 17, 4987–4992 (1978). [PubMed: 214106]
109. Steensgaard J, Humphries S, Spragg SP, in Preparative Centrifugation: A Practical Approach, Rickwood D, Ed. (IRL Press, 1992), pp. 187–232.
110. Wille H, Prusiner SB, Ultrastructural studies on scrapie prion protein crystals obtained from reverse micellar solutions. Biophys. J 76, 1048–1062 (1999). [PubMed: 9916037]
111. Fox BG, Blommel PG, Autoinduction of protein expression. Curr. Protoc. Protein Sci **Chapter 5**, Unit 5.23 (2009).
112. Kraus A, Saijo E, Metrick II MA, Newell K, Sigurdson CJ, Zanusso G, Ghetti B, Caughey B, Seeding selectivity and ultrasensitive detection of tau aggregate conformers of Alzheimer disease. Acta Neuropathol. 137, 585–598 (2019). [PubMed: 30570675]
113. Sanders DW, Kaufman SK, DeVos SL, Sharma AM, Mirbaha H, Li A, Barker SJ, Foley AC, Thorpe JR, Serpell LC, Miller TM, Grinberg LT, Seeley WW, Diamond MI, Distinct tau prion strains propagate in cells and mice and define different tauopathies. Neuron 82, 1271–1288 (2014). [PubMed: 24857020]
114. Collinge J, Clarke AR, A general model of prion strains and their pathogenicity. Science 318, 930–936 (2007). [PubMed: 17991853]

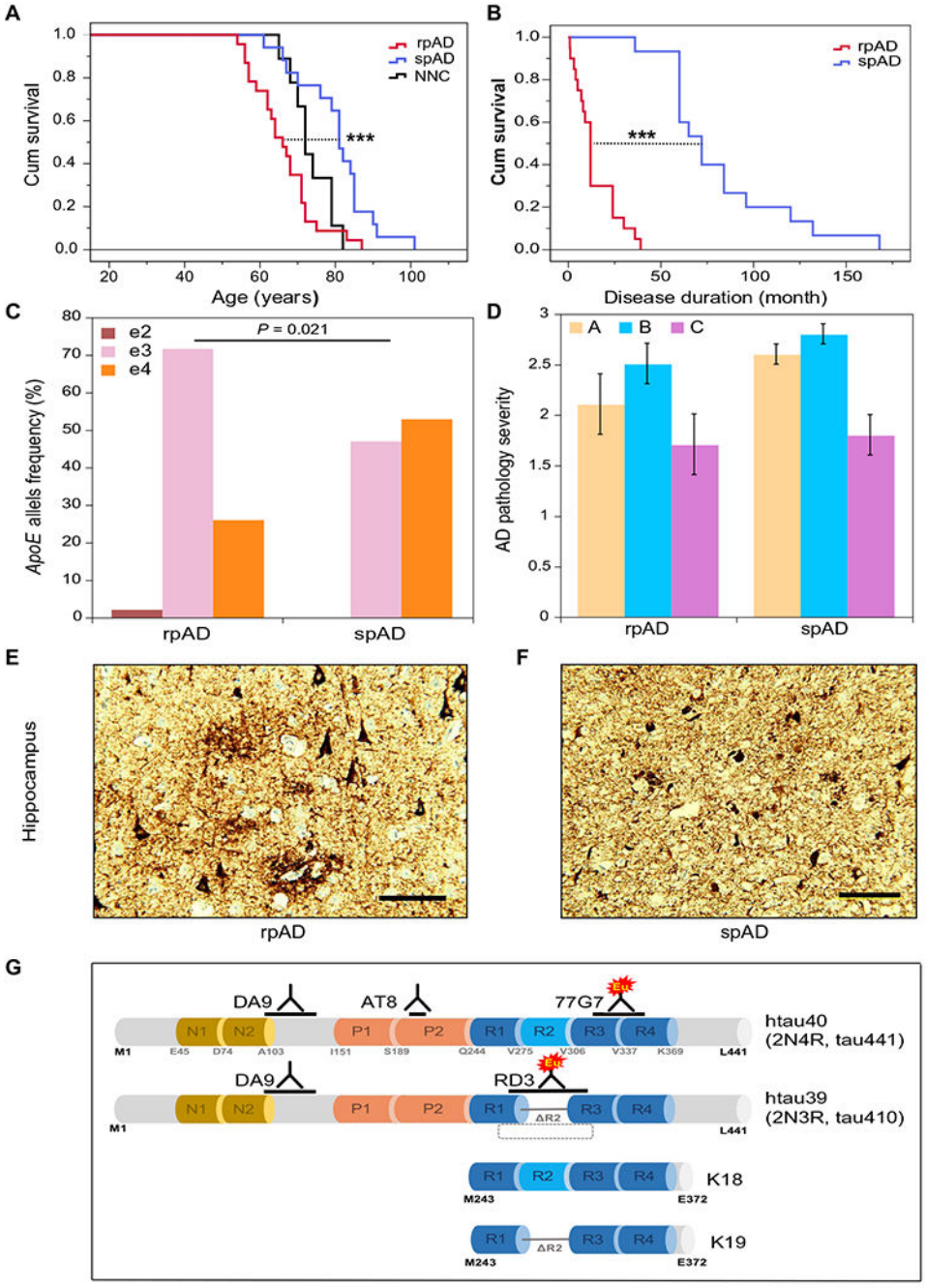

Fig. 1. Progression rates, *APOE* gene allelic frequency, neuropathology profiles, and Tau protein structure with tools for monitoring conformation and seeding potency of different isoforms in AD.

(**A**) Kaplan-Meier cumulative survival analysis and (**B**) duration of disease of cases with pathologically verified AD that were initially referred to National Prion Disease Pathology Surveillance Center with rapidly progressive dementia (rpAD, $n = 23$) and cases of slowly progressive AD (spAD; $n = 17$) collected at CWRU Alzheimer Research Center (9). NNC, non-neurologic controls. Statistical significance for difference in survival at *** $P < 0.001$ was determined with the log-rank (Mantel-Cox) and generalized Wilcoxon test.

(**C**) Frequency of e4 allele of *APOE* gene allelic polymorphisms in rpAD and spAD. Statistical significance was determined with two-tailed Fisher's exact test. (**D**) Severity of pathology classified according to National Institute on Aging–Alzheimer's Association (NIA-AA) guidelines for the neuropathologic assessment (35) in rpAD and spAD. (**E** and **F**) Representative sections of hippocampus of patient with rpAD (left) and spAD (right). Immunohistochemistry was performed with AT8 mAb. Scale bars, 100 μm. (**G**) Features within the TAU proteins and antibody epitopes; N, N-terminal acidic domain; P, proline-rich domain; R, microtubule-binding domains with four imperfect repeat regions separated by flanking sequences are not to scale, with microtubule-binding repeats exaggerated; C-terminal tail (gray); Eu, europium label.

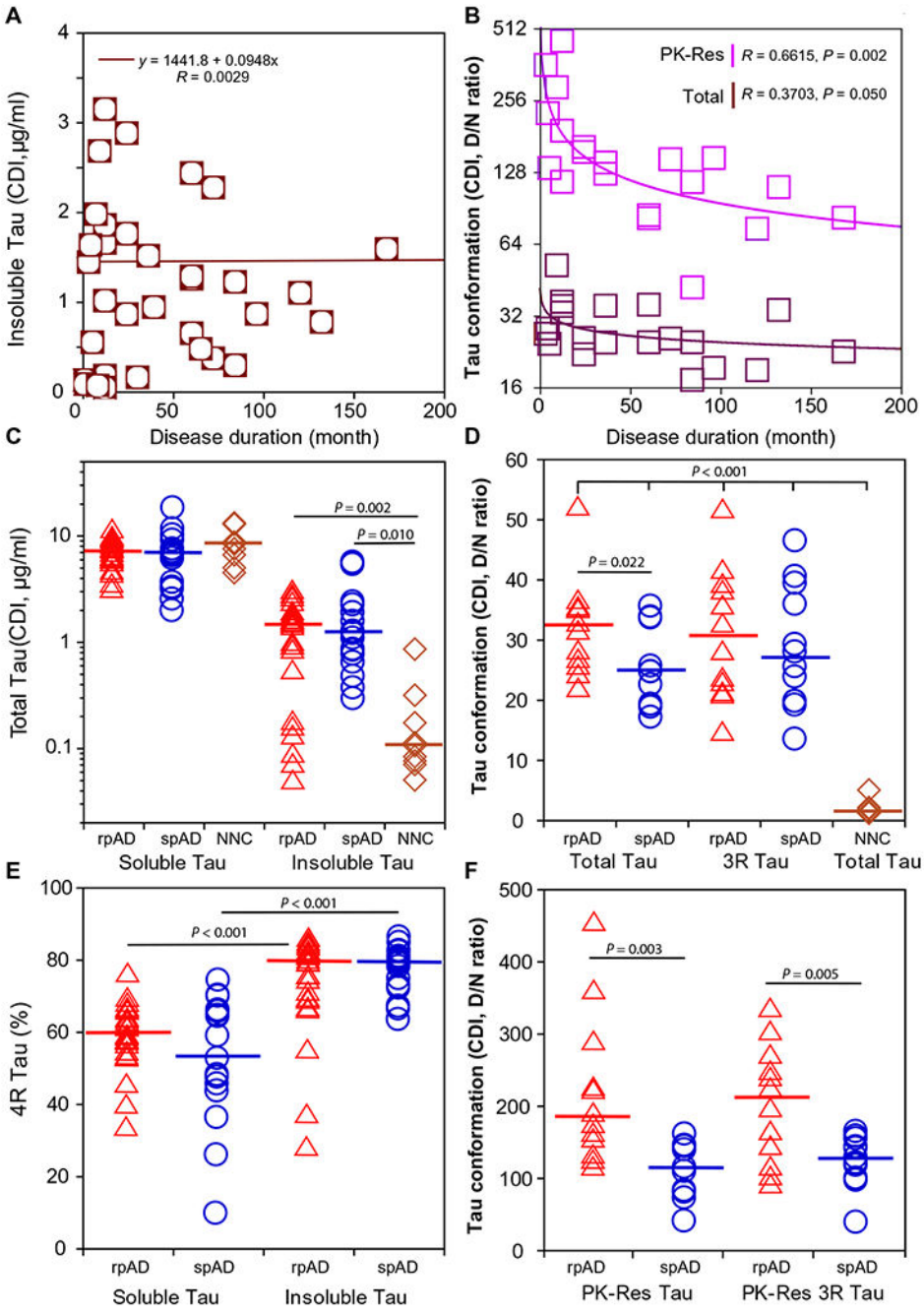

Fig. 2. Concentration and conformational profiles of TAU isoforms in the hippocampus of patients with AD and age-matched controls.

(**A**) Concentration of sarkosyl-insoluble TAU plotted as a function of disease duration. (**B**) Total TAU conformation (denatured/native CDI-D/N signal ratio) of sarkosyl-insoluble TAU before (Total) and after protease treatment (PK-Res). (**C**) Concentrations of detergent-soluble and insoluble total TAU in the hippocampus of rpAD and spAD cases and age-matched NNCs. (**D**) The diverse conformational profiles of total and 3R sarkosyl-insoluble TAU in rpAD, spAD, and NNC cases. (**E**) Fraction (%) of 4R TAU in the soluble and

insoluble TAU in rpAD and spAD. (**F**) The diverse conformational profiles of PK-Res sarkosyl-insoluble total TAU and 3R TAU in rpAD and spAD. The data were obtained with sandwich-formatted (before) and direct (after PK treatment) CDI to monitor R3,4 TAU domain (residues 316 to 355) with 77G7 mAb in native (N) and denatured (D) state of total TAU after unfolding with Gdn HCl; the 3R TAU was determined with RD3 mAb [epitopes 267 to 316 (99, 100)] (Fig. 1G). All measurements were performed in triplicate, and concentrations are expressed in ng/ml of 10% brain homogenate; horizontal lines in plots indicate medians, and statistical significance was determined with two-way ANOVA.

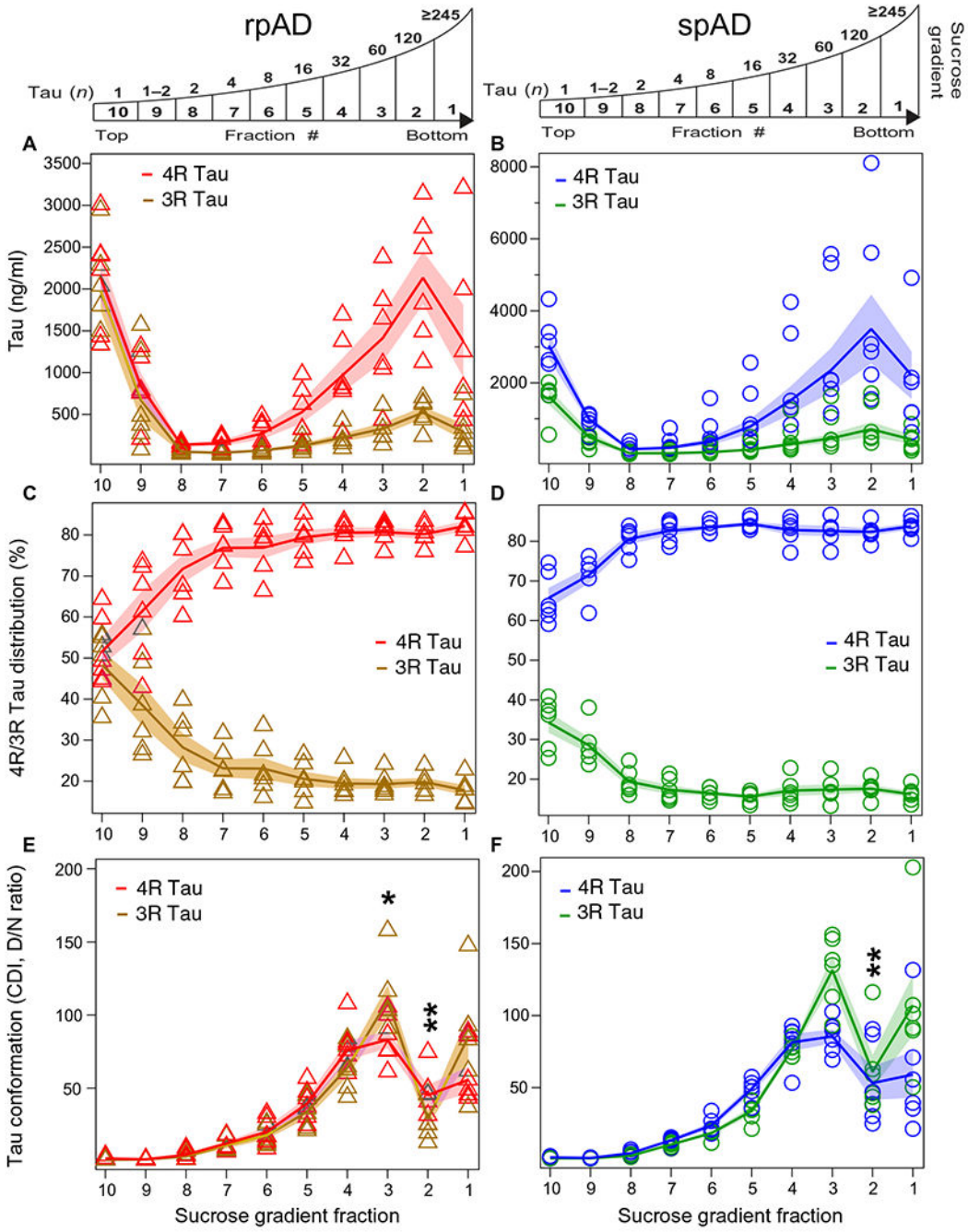

Fig. 3. Tau particles with different conformation and sizes composed of 4R and 3R TAU isoforms in the hippocampus of rpAD (A, C, E) and spAD (B, D, F) cases.

(**A** and **B**) Concentration of 4R and 3R TAU in sucrose gradient fractions. The samples were fractionated by sedimentation velocity using ultracentrifugation in sucrose gradient and analyzed by CDI for 4R and 3R TAU. The top panels are schematic representation of sedimentation velocity profile in sucrose gradient calibrated with standard proteins and recombinant 4R K18 and 3R K19 in monomeric and fibrillar state (fig. S1, E and F) TAU. (**C** and **D**) Relative distribution (%) of 4R and 3R TAU in sucrose gradient fractions of rpAD

and spAD cases. (**E** and **F**) Conformational profiling of 4R and 3R TAU in the sucrose gradient fractions of (E) rpAD and (F) spAD cases. The CDI was performed in duplicate or triplicate for each sucrose fraction of each AD case sample, and the line and shades are averages ± SEM. Statistical significance at $*P < 0.05$ and $**P < 0.01$ for the conformation of fractions 1, 2, and 3 was determined with ANOVA.

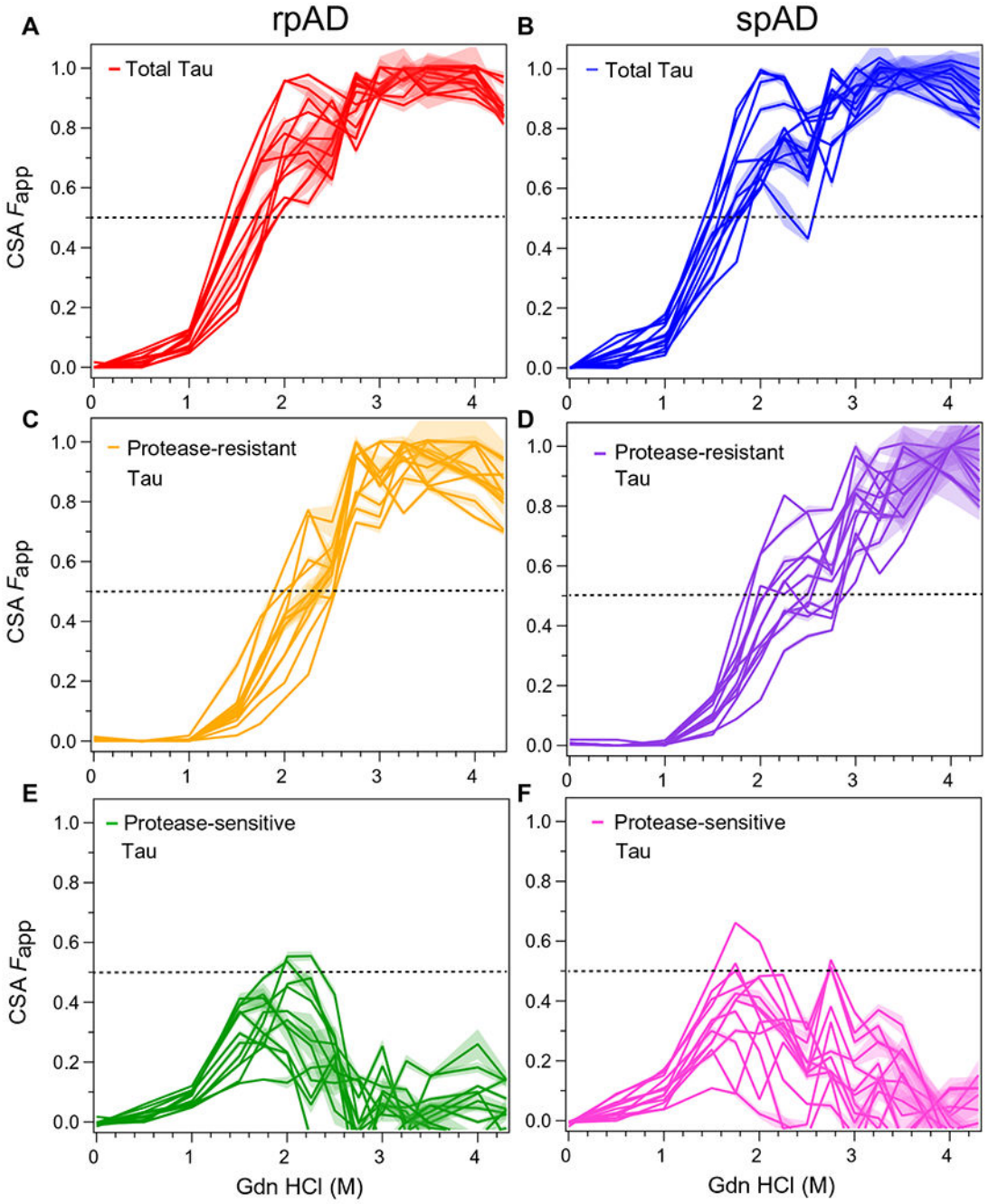

Fig. 4. Structural diversity and conformationally distinct subpopulations of total TAU in the hippocampus of AD determined directly in the brain tissue homogenate with CSA.

(**A**) Conformational stability curves of total hippocampal TAU in rpAD (n = 12), each curve representing dissociation and unfolding of TAU in an individual patient. (**B**) Conformational stability curves of total hippocampal TAU of individual spAD cases (n = 12). (**C**) Conformational stability curves of protease-resistant hippocampal TAU in rpAD (n = 12). (D) Conformational stability curves of protease-resistant TAU hippocampal TAU of individual spAD cases (n = 12). Differential stability curves of protease-sensitive

hippocampal TAU in (**E**) rpAD and (**F**) spAD. The lines and shades in the plots are mean ± SEM values of apparent fractional change (F_{app}) of each brain sample in the transition from native to denatured state obtained from triplicate measurements at each concentration of denaturant (Gdn HCl). The 50% of unfolded TAU expressed as midpoints of CSA F_{app}, [Gdn HCl]1/2, is illustrated with dashed lines.

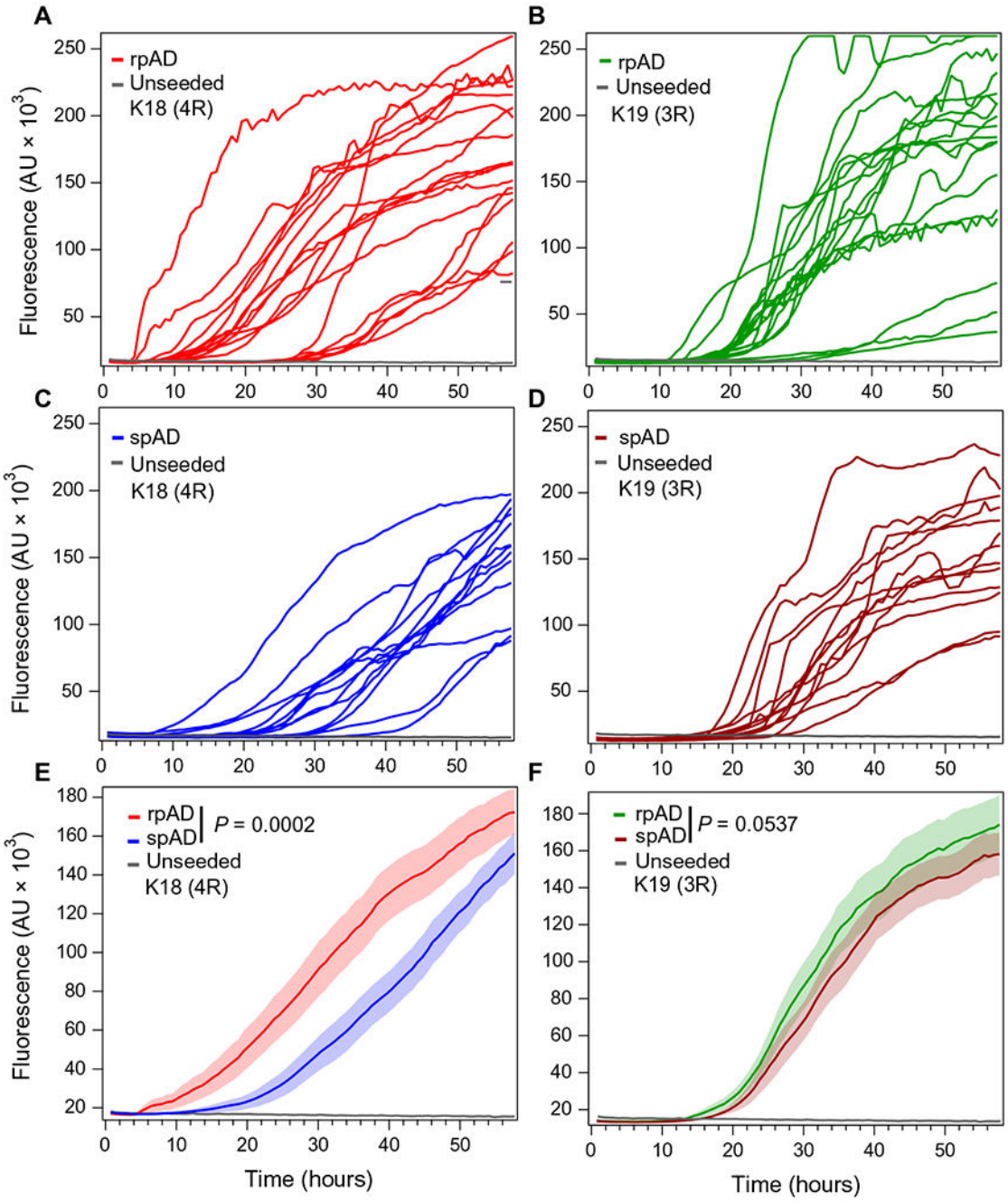

Fig. 5. Seeding response of K18 and K19 TAU substrates to hippocampus-derived TAU.

(**A**) K18 and (**B**) K19 TAU substrates seeded with 10^4-fold dilution rpAD ($n = 19$) brain samples and monitored in real time by thioflavin T fluorescence. (**C**) K18 and (**D**) K19 TAU substrates seeded with spAD ($n = 14$) brain samples diluted 10^4-fold and monitored in real time by thioflavin T fluorescence. (**E**) Averaged K18 and (**F**) K19 TAU substrate seeding response with rpAD ($n = 19$) and spAD ($n = 14$) brain samples. All samples were diluted 10^4-fold, and the curves are averages of thioflavin T florescence intensity in four wells at a given time point; unseeded K18 and K19 TAU constructs were applied as negative controls

of spontaneous aggregation. The rpAD and spAD seeding kinetic curves were compared by the two-tailed log-rank (Mantel-Cox) and two-tailed generalized Wilcoxon test. AU, arbitrary units.

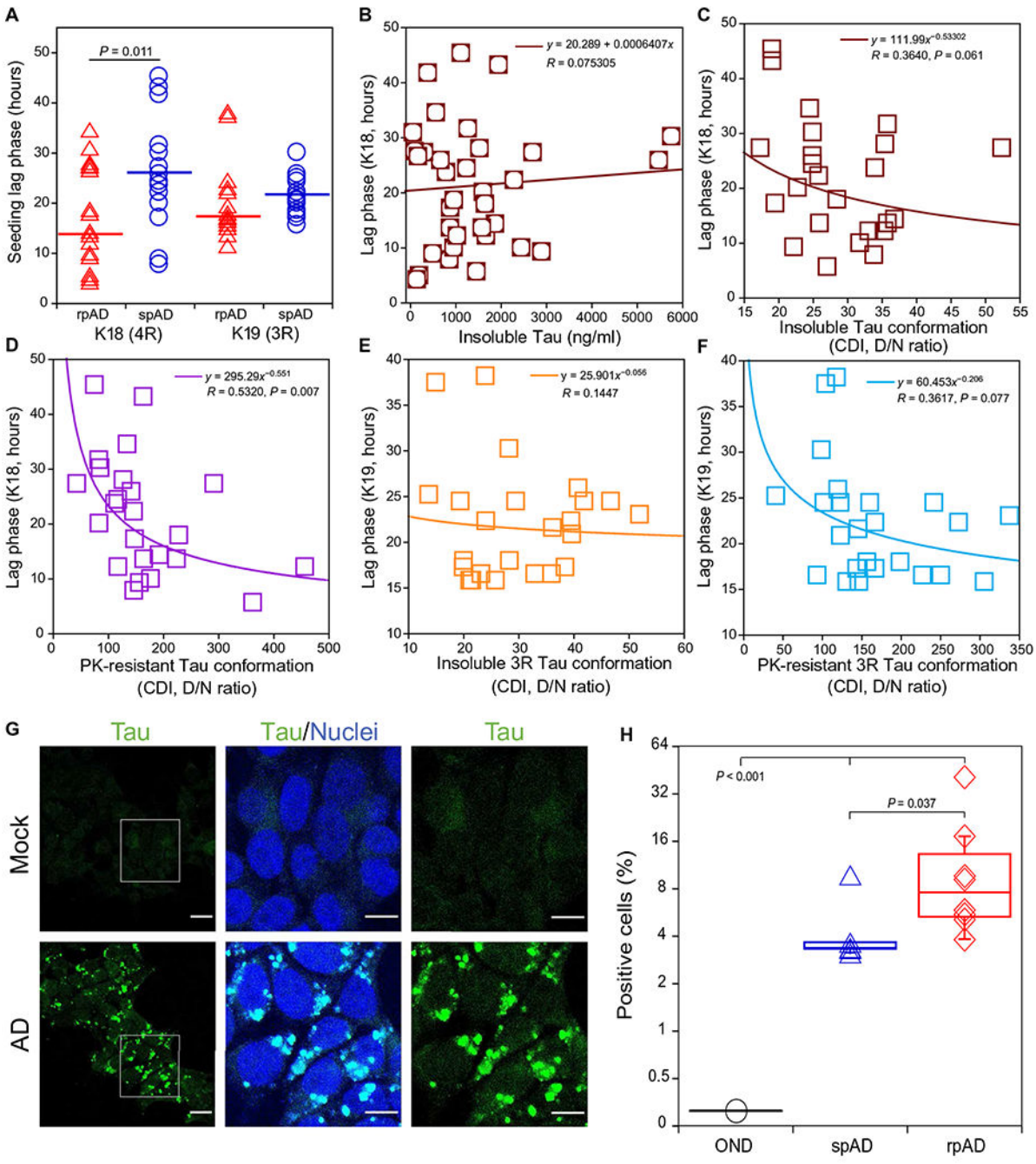

Fig. 6. Seeding potency and replication rates of different conformers of TAU.

(**A**) Lag phase of seeding K18 (4R) and K19 (3R) TAU substrates with hippocampal TAU accumulating rpAD (n = 19) and spAD (n = 14). (**B**) Specific seeding activity expressed in hours of lag phase per nanogram of misfolded sarkosyl-insoluble TAU accumulating in rpAD and spAD. Regression analysis of seeding lag time with K18 (4R) TAU substrate and conformations of (**C**) insoluble TAU and (**D**) protease-resistant TAU in the hippocampus of AD cases expressed by CDI D/N ratios of total and 3R TAU (n = 33). Regression analysis of seeding lag time with K19 (3R) TAU substrate and conformations of (**E**) insoluble TAU and

(**F**) protease-resistant TAU in the hippocampus of AD cases expressed by CDI D/N ratios of total and 3R TAU (n = 33). The lag phase of each sample is an average of four seeding assays at 10^4-fold dilution of brain samples, and the CDI was performed in triplicate in the same samples. (**G**) Cell seeding activity of phosphotungstic acid (PTA)-precipitated AD brain TAU aggregates in HEK-TAURD-LM-YFP reporter cells was imaged for 5 days after seeding. Scale bars, 40 and 20 μm in the boxed images. (**H**) Average frequency of positive cells exposed to PTA-precipitated TAU from spAD (n = 5) and rpAD cases (n = 8) and other neurological disease control (OND); each brain-derived sample was evaluated in 15 wells, both blindly and with automated Aiforia AI software. Each box encloses 50% of the data with median value displayed as a line; whiskers mark the minimum and maximum, and individual points indicate an outlier value outside the UQ + 1.5*IQR interval, where UQ is upper quartile and IQR is interquartile range.

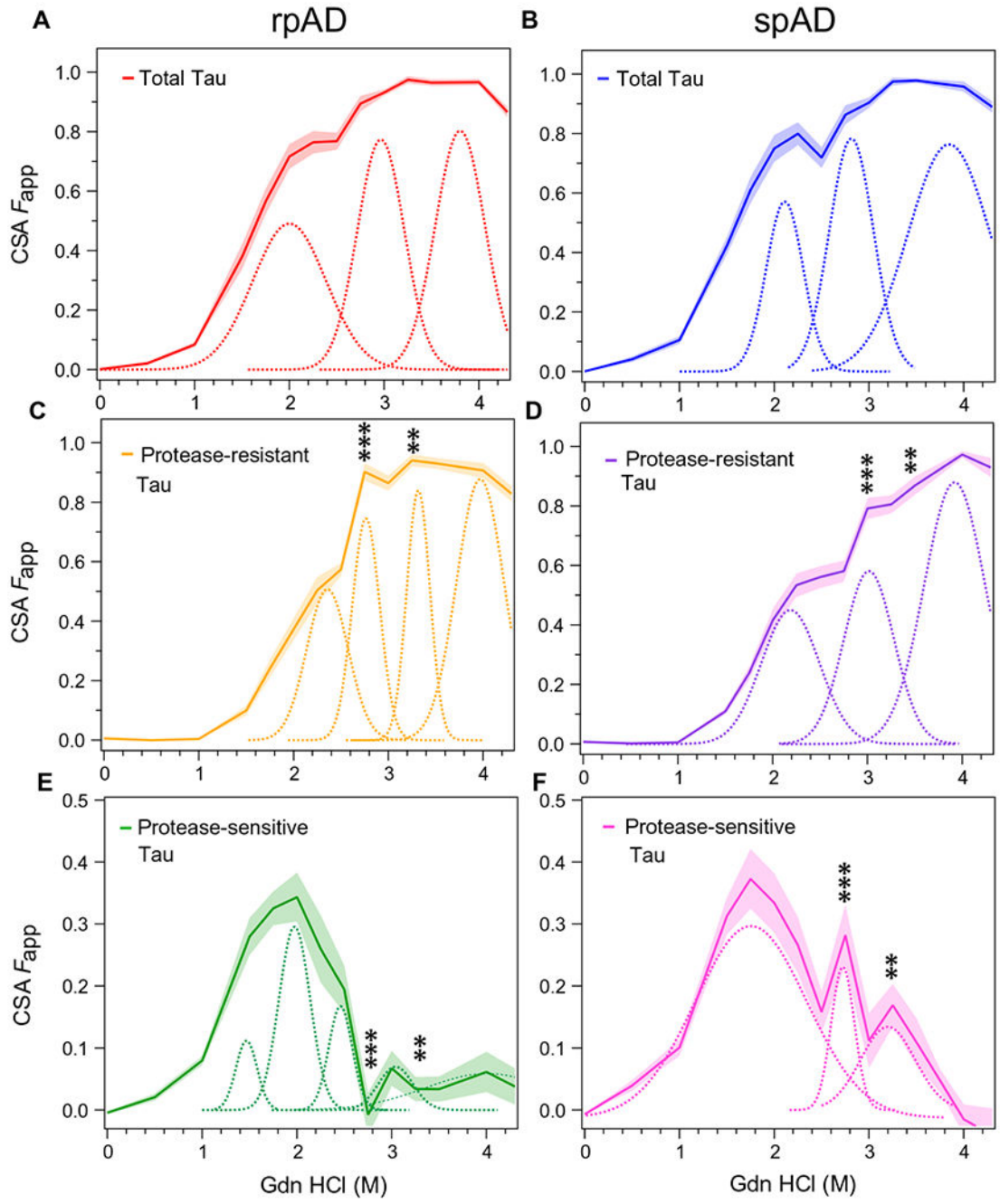

Fig. 7. Conformational profiles of detergent-insoluble, protease-resistant, and protease-sensitive total TAU averaged in AD cases with different progression rates.

Averaged CSA profiles and statistical mechanical Gaussian peak deconvolution of sarkosyl-insoluble total TAU in (**A**) rpAD and (**B**) spAD. Averaged CSA profiles of protease-resistant total TAU in (**C**) rpAD and (**D**) spAD. Conformational profiles of protease-sensitive total TAU in (**E**) rpAD and (**F**) spAD. We used the deconvolution of averaged CSA profiles with a multiple peak Gaussian model to identify common components in the CSA curves and the Gdn HCl concentration at the maximum peak height. Using these peak-derived Gdn HCl

values, the CSA F_{app} values at a given Gdn HCl concentration were compared in individual rpAD and spAD cases using two-tailed ANOVA. The statistical significance was determined with generalized Wilcoxon tests and ANOVA for data at each denaturant concentration (***$P < 0.0001$ and **$P < 0.003$).

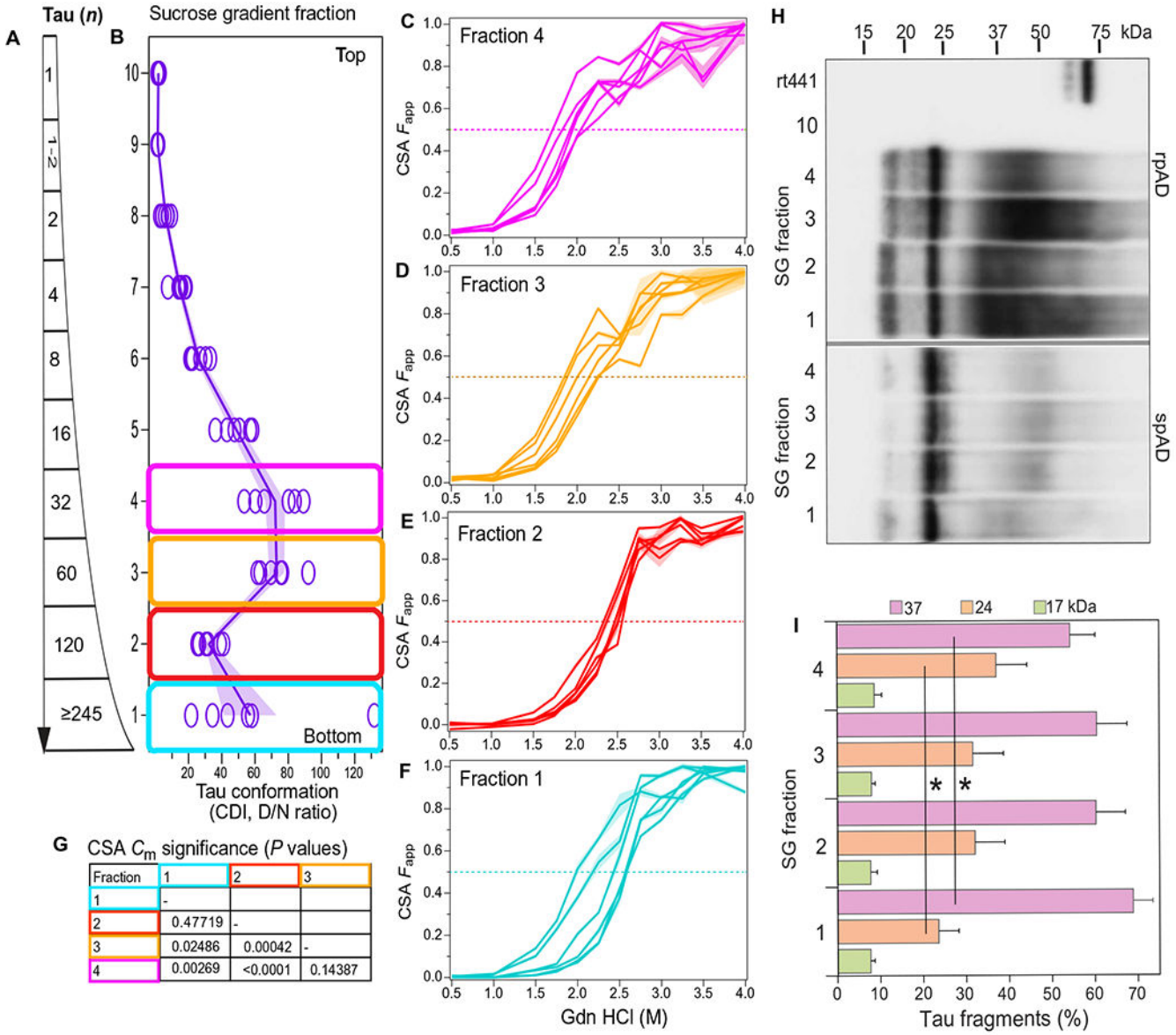

Fig. 8. Conformational signatures of TAU particles with different sizes fractionated by sedimentation velocity using ultracentrifugation in sucrose gradient and analyzed by CSA and limited trypsin digestions.

(**A**) Schematic representation of sedimentation velocity profile in sucrose gradient calibrated with standard proteins and recombinant K18 and K19 TAU. (**B**) Conformational profiling of 4R TAU in the sucrose gradient with CDI followed by (**C** to **F**) CSA of each fraction and (**G**) statistical comparison of different fractions using the midpoint of Gdn HCl denaturant concentration (C_m). (**H**) Representative Western blots of sucrose gradient fractions after trypsin digestion and developed with mAb A16040D (epitopes 269 to 281). (**I**) The densitometry of major trypsin-resistant TAU core bands in each fraction of AD cases (n = 6). Each CSA was performed in triplicate, and the plots are averages ± SE in shade.

Statistical significance for the densitometry and conformation (C_m) of fractions 1, 2, 3, and 4 was determined with ANOVA. $*P < 0.05$.